



## Synthesis, melt molding and hydrolytic degradation of poly(*L*-lactide-*co*-*L*-methylglycolide) and its composites with carbonated apatite



Alexander N. Tavtorkin <sup>a</sup>, Egor A. Kretov <sup>a,b</sup>, Maria P. Ryndyk <sup>a,b</sup>, Ilya E. Nifant'ev <sup>a,b,c,\*</sup>, Andrey V. Shlyakhtin <sup>a,c</sup>, Vladimir V. Bagrov <sup>a,c</sup>, Alexander A. Vinogradov <sup>a</sup>, Pavel V. Ivchenko <sup>a,c,\*</sup>

<sup>a</sup> A. V. Topchiev Institute of Petrochemical Synthesis RAS, Leninsky pr. 29, 119991 Moscow, Russian Federation

<sup>b</sup> National Research University Higher School of Economics, Faculty of Chemistry, Vavilova st. 7, 117312 Moscow, Russian Federation

<sup>c</sup> Department of Chemistry, M. V. Lomonosov Moscow State University, Leninskie Gory 1–3, 119991 Moscow, Russian Federation

### ARTICLE INFO

#### Keywords:

Carbonated apatite  
Composite  
Methylglycolide  
PLGA  
Ring-opening polymerization

### ABSTRACT

Poly(lactic-*co*-glycolic acid)s (PLGAs) hold considerable significance for their biomedical applications. Biodegradation and mechanical properties of PLGAs and PLGA-based composites are strongly influenced by lactate/glycolate (L/G) ratio in copolymers, molecular weight characteristics and microstructure of PLGAs. The common approach to PLGAs is based on ring-opening copolymerization of lactides and glycolide, the products of which contain long (L)<sub>n</sub> and (G)<sub>n</sub> segments. An efficient but expensive approach to PLGAs with given L-G sequences is a segment assembly polymerization that is hardly applicable for the synthesis of high-MW PLGAs. In the present work, for the first time we synthesized lactate-enriched PLGAs using ring-opening copolymerization of *L*-lactide (*L*-LA) with *L*-methylglycolide (*L*-MeGL) in 85:15 and 70:30 molar ratios, resulting in *L*-PLMG 85/15 and *L*-PLMG 70/30 copolymers. *L*-PLGA 85/15 with the same L/G ratio as in PLMG 70/30 was synthesized by ring-opening copolymerization of *L*-LA with glycolide as a sample for a comparison. According to <sup>1</sup>H and <sup>13</sup>C NMR data and [α]<sub>D</sub> measurements, *L*-MeGL-based PLGAs had a unique microstructure, e.g. macromolecules of *L*-PLMG 85/15 consisted of L<sub>n</sub> sequences with single G insertions. Composites of PLLA and three samples of PLGAs with plate-like carbonated apatite (pCap) containing 25 and 50 wt.% of the filler were prepared. Rectangular specimens from (co)polymers and (co)polymer composites were obtained by injection molding and studied. Due to the absence of highly reactive (G)<sub>n</sub> fragments, *L*-PLMG 85/15 and PLMG 70/30-based materials demonstrated higher thermal and hydrolytic stability, mechanical testing showed that *L*-MeGL-based copolymers provide better maintaining of the bending strength in comparison with *L*-PLGA 85/15 matrix.

### 1. Introduction

The very complex structure of the human bone comprises a triple helix tropocollagen macromolecules, self-assembled into collagen fibrils, nano-sized plate-like crystallites of bone apatite (BA), and osteopontin as a natural compatibilizer for BA and collagen [1,2]. The knowledge about the nature of bone were the starting point of the bionic design of composite bone substitutes in which synthetic biodegradable polymers serve as a matrix, and synthetic bone mineral substitutes (BMSs) serve as a filler [3–6]. In recent decades, bone surgery and orthopedics has reached a qualitatively new level through the implementation of biodegradable polymers and BMSs in medical devices [7,8].

Calcium phosphate ceramics (CPCs) containing Ca<sup>2+</sup>, PO<sub>4</sub><sup>3-</sup> and other biocompatible cations and anions are seen as a promising BMSs. In most of works, FDA approved [9] hydroxyapatite (HAp) was studied as a BMS [3–5,10–12]. However, pure "stoichiometric" HAp Ca<sub>10</sub>(PO<sub>4</sub>)<sub>6</sub>(OH)<sub>2</sub> is not quite appropriate because its high degree of crystallinity and reduced biodegradability [13,14]. More chemically active inorganic phases, e.g. β-tricalcium phosphate [15], octacalcium phosphate [16], biphasic calcium phosphate [17] and the like [18] have been studied as a BMSs. Carbonated apatite (Cap) is most similar in its chemical composition to BA and is attractive due to basic character of Cap [14,19]. In 2017 Cap was approved as a BMS by the Pharmaceuticals and Medical Devices Agency of Japan [14], and in recent years Cap-based scaffolds for bone surgery and orthopedics have attracted increasing

\* Correspondence author at: 119991, Leninskie Gory, 1–3, Moscow, Russian Federation

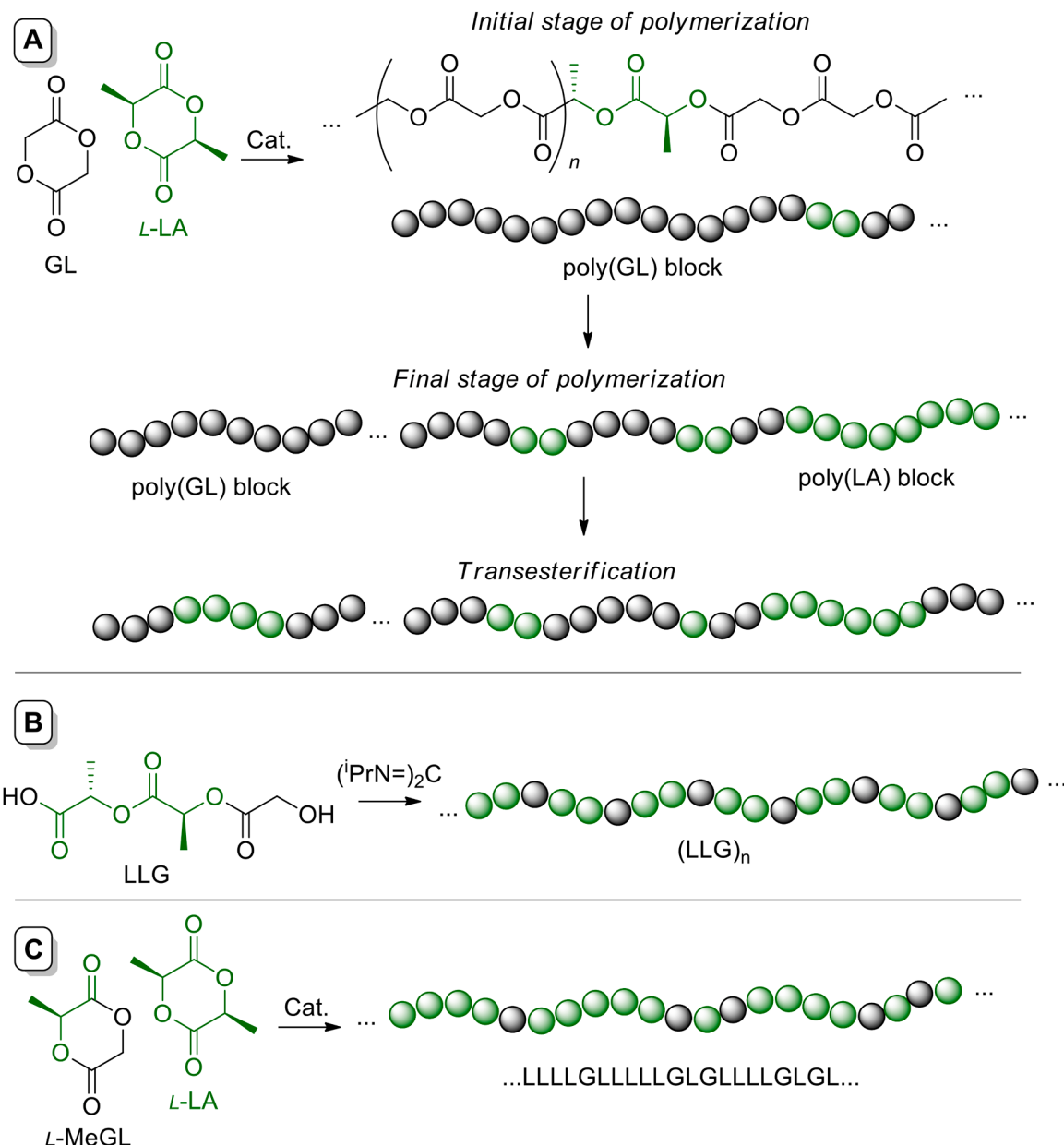
E-mail address: [ilnif@yahoo.com](mailto:ilnif@yahoo.com) (I.E. Nifant'ev).

scientific attention [14,20–31]. However, polyester/CAp composites are less investigated [32–36]. Rare applications of CAp in composite formulations may be due to insufficient study of the synthetic approaches to perfectly shaped nano-/microsized CAp materials [37–39]. Three years ago, we have developed hydrothermal method of the synthesis of well-shaped CAp crystallites [40]. During the further studies, we showed that in comparison with other CPCs plate-like CAp (pCAp) demonstrate better potential for using as a BMS [41] and higher biocompatibility [42].

Among biodegradable polymers, synthetic polyesters are attractive materials for the preparation of composites for bone repair. Poly(*L*-lactide) (PLLA, Scheme 1A) is one of the best-known polyesters; PLLA is biocompatible and can be subjected to melt molding [5,43,44]. However, PLLA does not fulfill the specific requirements to polymers designed for biomedical applications, its use is complicated by poor toughness, slow degradation and hydrophobicity. The introduction of more reactive and hydrophilic glycolic acid (GA) comonomer unit into

the PLLA chain with a formation of poly(lactic-co-glycolic acid)s (PLGAs, Scheme 1A) allows to fine-tune the hydrophilicity and degradation rate of the polymer by varying the lactate/glycolate (L/G) molar ratio [45,46], widening the area of applications of PLGAs [6,8,46–48]. In particular, glycolate-enriched PLGA 10/90 is widely used as a suture material [49], whereas PLGA 85/15 has been successfully applied in the manufacture of plates, screws, pins and other surgical products [50]; both of these PLGA formulations are also FDA approved [7,51].

The synthesis of high-MW PLLA and PLGAs is based on ring-opening polymerization (ROP) of cyclic diesters, *L*-lactide (*L*-LA) and glycolide (GL, Scheme 1A). However, reactivities of *L*-LA and GL in ROP differ significantly, which leads to the formation of gradient copolymers containing long poly(GL) segments at the initial stage of polymerization and long poly(*L*-LA) segments at the end of the process (Scheme 1A) [52]. Preparation of random copolymers is achieved by using low-active catalysts, e.g. tin(II) 2-ethylhexanoate ( $\text{Sn}(\text{Oct})_2$ ), and elevated temperatures; randomization is achieved by transesterification. Note that



**Scheme 1.** (A) Conventional synthesis of PLGAs [52]. (B) Segmer assembly polymerization approach to PLGAs with controlled microstructure [56]. (C) Preparation of highly statistical PLGAs using *L*-MeGL (this work).

highly statistical PLGA can be hardly obtained by this method, for example, copolymerization of 1:1 *L*-LA/GL mixture using Sn(Oct)<sub>2</sub> at 110 °C after 1 week resulted in copolymer with the average sequence lengths for lactic (*L<sub>L</sub>*) and glycolic (*L<sub>G</sub>*) units of 9.6 and 8.6 [53]. As was shown in [54], even lactate-enriched 85/15 *L*-PLGA contained hydrophilic and highly reactive oligo(GL) fragments.

In 2008, Meyer and coll. proposed the segment assembly polymerization (SAP) approach for the control of PLGA microstructure [55]. This approach is based on the synthesis of oligomeric hydroxy acids with a given lactate/glycolate sequences followed by the formation of polyesters under the action of carbodiimides, a number of PLGAs with strictly defined microstructures was obtained [56] (see example in Scheme 1B). However, this approach is relatively labor-intensive and seems hardly applicable for the synthesis of high-MW PLGAs (the highest reported *M<sub>n</sub>* value of SAP PLGA was ~42 kDa [56]).

Cyclic diester combining glycolate and lactate fragment in its structure, 3-methyl-1,4-dioxane-2,5-dione (methylglycolide, MeGL), can be considered as a comonomer that allows to insert lactate fragments to glycolate-enriched PLGA formulations or glycolate fragments to lactate-enriched PLGAs with higher level of randomization due to its reactivity that occupies the middle ground between GL and LA (e.g. the reactivities of *rac*-MeGL relative to GL and *rac*-LA at 140 °C with the use of Sn(Oct)<sub>2</sub> catalyst were found to be 0.50 and 1.86, respectively [57]). However, the most of the studies were devoted to the synthesis of alternating PLGAs 50/50 with the use of *rac*-MeGL in 1990s – early 2000s [58–60] and *L*-MeGL in recent years [61–64]. To date, only copolymerization of MeGL with GL was studied [52,65], the use of MeGL in the synthesis of lactate-enriched PLGAs remains unexplored. In recent patent [66] copolymerization of *rac*-MeGL with lactide, initiated by Sn(Oct)<sub>2</sub> and OH-terminated polystyrene, was described on the only single example without characterization of copolymer obtained.

The goals of our research were to study copolymerization of *L*-MeGL with *L*-LA, to investigate the microstructure and properties of copolymers, to prepare PLGA-based composite materials with the use of pCap as an inorganic filler, and to explore hydrolytic degradation of PLGAs and PLGA-based composites in terms of mechanical properties of molded samples and molecular weight characteristics of PLGA matrix.

## 2. Experimental section

### 2.1. Materials, solvents and reagents

All solvents were supplied by Merck (Darmstadt, Germany). Toluene, diethyl ether, tetrahydrofuran (THF), and triethylamine were refluxed with Na/benzophenone/dibenzo-18-crown-6 and distilled prior to use. Acetonitrile was stored over K<sub>2</sub>CO<sub>3</sub>, refluxed, and distilled from CaH<sub>2</sub>. Hexane was refluxed for 10 h over sodium and then distilled and stored in an argon atmosphere over sodium. Methanol was refluxed and distilled from magnesium methoxide. Sn(Oct)<sub>2</sub>, potassium *tert*-butoxide, acetic acid (AcOH), NaNO<sub>2</sub>, CaCO<sub>3</sub>, Na<sub>2</sub>CO<sub>3</sub>, NaHCO<sub>3</sub>, Na<sub>2</sub>HPO<sub>4</sub>·12H<sub>2</sub>O, isopropanol, *n*-pentane, *L*-alanine, 2-bromoacetyl bromide, N-ethyl-N-isopropylpropan-2-amine, phosphate-buffered saline (PBS) containing 0.131 mol/L NaCl and 0.0027 mol/L KCl (Merck), 1-Octadecanol (stearyl alcohol, 99%, Shanghai Macklin Biochemical Technology Co., Ltd, Zhangjiang, China), deuterated solvents CDCl<sub>3</sub> and DMSO-d<sub>6</sub> (D 99.8 at.%, Cambridge Isotope Laboratories, Inc., Tewksbury, MA, USA) were used as purchased. *L*-LA (Merck) was purified by double recrystallization from toluene, followed by sublimation at 0.1 Torr; [α]<sub>D</sub> = -295.7° (1.0 g·dL<sup>-1</sup>, toluene, 25 °C) (lit. [α]<sub>D</sub> = -298.8° (1.0 g·dL<sup>-1</sup>, toluene, 20 °C) [67]). GL (Merck) was washed with dry toluene and sublimated. *L*-Lactic acid (80%) was evaporated under reduced pressure and distilled in vacuo. Commercial PLLA (*M<sub>n</sub>*107 kDa, *D<sub>M</sub>* 2.02, supplied by FDplast, Moscow, Russia) was chosen as a polyester component for comparison.

(*S*)-3-Methyl-1,4-dioxane-2,5-dione (*L*-methylglycolide, *L*-MeGL) was synthesized using modified method described previously [61,68]

(for details see Section S1 in the Appendix A). [α]<sub>D</sub> = -223.6° (1.0 g·dL<sup>-1</sup>, CHCl<sub>3</sub>, 25 °C) (lit. [α]<sub>D</sub> = -220.5° (1.0 g·dL<sup>-1</sup>, CHCl<sub>3</sub>, 0 °C) [62]).

### 2.2. Analysis

The <sup>1</sup>H and <sup>13</sup>C {<sup>1</sup>H} NMR spectra were recorded on a Bruker AVANCE 400 spectrometer (400 MHz, Bruker Corporation, Billerica, MA, USA) at 20 °C. The chemical shifts are reported relative to the solvent residual peaks (CDCl<sub>3</sub>: δ = 7.26 ppm for <sup>1</sup>H NMR spectra and 77.16 ppm for <sup>13</sup>C NMR spectra; DMSO-d<sub>6</sub>: δ = 2.50 ppm for <sup>1</sup>H NMR spectra and 39.52 ppm for <sup>13</sup>C NMR spectra).

Scanning electron microscopy (SEM) images and energy dispersive X-ray (EDX) analysis data were obtained using a Phenom XL microscope (Thermo Fisher Scientific, Waltham, MA, USA) at an accelerating voltage of 5.0 kV.

X-ray diffraction (XRD) powder patterns were recorded using a MiniFLEX 600 powder diffractometer (Rigaku Corp., Tokyo, Japan) equipped with a Cu-Kα<sub>1,2</sub> (λ = 1.5418 Å) X-ray tube and a 1D D/teX position-sensitive detector. Data were collected at room temperature in the 2θ range 4.5°–90° with a 0.02° step size using a Bragg–Brentano setup. The cell parameters were determined by full-profile fitting, as implemented in Bruker TOPAS 5 (Bruker Corp., Billerica, MA, USA).

Fourier transform infrared (FT-IR) spectra were recorded using IROS 05 spectrometer (Simex LTD, Novosibirsk, Russia) equipped with sample holder with diamond prism in the attenuated total reflection (ATR) mode. Experimental parameters: spectral range 500–4000 cm<sup>-1</sup>, resolution 2 cm<sup>-1</sup>, 15 scans.

Specific optical rotation ([α]<sub>D</sub>) of the monomers and copolymers were measured at a concentration of 1.0 g dL<sup>-1</sup> using a AP-300 polarimeter (ATAGO Co. Ltd., Tokyo, Japan; cell length 20 cm) at a wave length of 589 nm. Every measurement was repeated five times.

Size exclusion chromatography (SEC) measurements were performed in THF (40 °C, flow rate 1 mL/min) on a 1260 Infinity II (Agilent Technologies, Santa Clara, CA, USA) integrated instrument equipped with a PLgel MIXED-A column (1 × 10<sup>3</sup> – 4 × 10<sup>7</sup> Da), an autosampler, and a refractive index detector. The measurements were recorded with universal calibration according to a polystyrene standard.

Differential scanning calorimetry (DSC) experiments were performed on the TGA/DSC1 apparatus (Mettler Toledo, Columbus, OH, USA). The samples were heated from 30 °C to 200 °C (1st heating) and kept at 200 °C for 3 min to eliminate the thermal history, then cooled to 30 °C and finally heated to 200 °C again (2nd heating). The rate of heating and cooling was 5 K·min<sup>-1</sup>.

Mechanical studies were carried out on tensile machine I1140M-5-01-1 (Tochpribor-KB LLC, Ivanovo, Russian Federation). Bending tests were conducted according to ISO 178:2010 by three-point deformation of the plates (60 × 10 × 1 mm, the distance between low points 25 mm). Flexural rate was 2 mm·min<sup>-1</sup>.

### 2.3. Synthesis of plate-like carbonated apatite (pCap)

The synthesis of pCap was conducted using modified method described previously [40,41]. NaHCO<sub>3</sub> (84.06 g, 1 mol) and KH<sub>2</sub>PO<sub>4</sub> (81.65 g, 0.6 mol) were placed into 1.8 L autoclave. CaCO<sub>3</sub> (100.1 g, 1 mol) and Na<sub>2</sub>[EDTA]·2H<sub>2</sub>O (372 g, 1 mol) were dissolved in distilled water (1 L). The solution was filtered into autoclave, after addition of water to the total volume of 1.6 L the autoclave was heated to 140 °C within 2 h and was kept at 140 °C within 24 h. After cooling to 20 °C, the precipitate was separated by decantation, washed by H<sub>2</sub>O (2 × 300 mL), isopropanol (2 × 200 mL), *n*-pentane (2 × 100 mL) and dried in vacuo. The yield was 20.2 g (21.2%). The resulting sample of pCap was analyzed by XRD, FT-IR spectroscopy and TGA (see Section 3.1 and Section S1.2 in the Appendix A).

## 2.4. Synthesis of copolymers

### 2.4.1. General polymerization procedure

Before polymerization experiments, stock solution of Sn(Oct)<sub>2</sub> (80 mg in 4.0 mL of toluene) was prepared. The calculated amounts of comonomers, stearyl alcohol and stock solution of Sn(Oct)<sub>2</sub> were placed under argon atmosphere into flame-dried flask. The flask was connected to vacuum line, and evacuated to a pressure of 0.02 Torr at 25 °C. After closing the vacuum tap, the flask was placed to oil bath, heated to 170 °C. After 8 h of heating, the polymer was extracted from the flask manually.

### 2.4.2. Copolymer of *L*-LA and GL, 85 mol.% *L*-LA (*L*-PLGA 85/15)

Prepared from *L*-LA (132.02 g, 916 mmol) and GL (18.80 g, 162 mmol) in the presence of stearyl alcohol (233 mg, 0.86 mmol) and Sn(Oct)<sub>2</sub> (21.9 mg, 0.054 mmol). The yield was 121 g (81%). <sup>1</sup>H NMR (CDCl<sub>3</sub>, 25 °C, 400 MHz) δ: 5.20 (q), 5.16 (q, 3 J = 7.1 Hz) {5.7H}; 4.91–4.64 (group of signals, 2H); 1.58 (d, 3 J = 7.1 Hz, 17H).  $\alpha_D^{20}$  (1.0 g·dL<sup>-1</sup>, CHCl<sub>3</sub>, 25 °C) = -139.9°

### 2.4.3. Copolymer of *L*-LA and *L*-MeGL, 85 mol.% *L*-LA (*L*-PLMG 85/15)

Prepared from *L*-LA (96.6 g, 670 mmol) and *L*-MeGL (15.3 g, 118 mmol) in the presence of stearyl alcohol (170 mg, 0.63 mmol) and Sn(Oct)<sub>2</sub> (16.0 mg, 0.039 mmol). The yield was 98 g (88%). <sup>1</sup>H NMR (CDCl<sub>3</sub>, 25 °C, 400 MHz) δ: 5.20 (q), 5.16 (q, 3 J = 7.1 Hz) {12.3H}; 4.88 (d, 2 J = 15.9 Hz, 1H); 4.88 (d, 2 J = 15.9 Hz, 1H); 1.58 (d, 3 J = 7.1 Hz, 34H).  $\alpha_D^{20}$  (1.0 g·dL<sup>-1</sup>, CHCl<sub>3</sub>, 25 °C) = -148.4°

### 2.4.4. Copolymer of *L*-LA and *L*-MeGL, 70 mol.% *L*-LA (*L*-PLMG 70/30)

Prepared from *L*-LA (80.0 g, 555 mmol) and *L*-MeGL (31.1 g, 239 mmol) in the presence of stearyl alcohol (170 mg, 0.63 mmol) and Sn(Oct)<sub>2</sub> (16.2 mg, 0.040 mmol). The yield was 95 g (86%).

<sup>1</sup>H NMR (CDCl<sub>3</sub>, 25 °C, 400 MHz) δ: 5.20 (q), 5.16 (q, 3 J = 7.1 Hz) {5.7H}; 4.88 (d, 2 J = 15.9 Hz, 1H); 4.65–4.59 (gr. d, 1H); 1.58 (d, 3 J = 7.1 Hz, 17H).  $\alpha_D^{20}$  (1.0 g·dL<sup>-1</sup>, CHCl<sub>3</sub>, 25 °C) = -147.5°

<sup>1</sup>H NMR spectra of copolymers are presented in Section S2 in the Appendix A.

## 2.5. Preparation of (co)polymer and composite samples

### 2.5.1. Molding of (co)polymer samples

The sample of PLLA or copolymer (10 g) was grafted into small pieces (1–3 mm) and placed into HAAKE MINIJet Pro (Thermo Fisher Scientific, Waltham, MA, USA) injection molding machine. Molding of the samples was made with the pressure of 600 Bar, the temperatures of molding were 180 °C (cylinder) and 50 °C (mold). A Mould HAAKE MINIJet 60 × 10 × 1 mm injection mold was used for casting of the samples for a bending test.

### 2.5.2. Molding of the composite samples

The sample of PLLA or copolymer (9 g) was dissolved in THF (50 mL). pCap (3 or 9 g) was added, after 1 h of stirring at 50 °C the mixture was poured into a PTFE cuvette and dried at 25 °C within 24 h. The film was chopped up into small pieces (1–3 mm) that were dried at 70 °C and 0.01 Torr within 1 h. Molding of the samples was made with the pressure of 600 Bar, the temperatures of molding were 185–190 °C (cylinder) and 50 °C (mold).

## 2.6. The studies of hydrolytic degradation of (co)polymer and composite samples

Hydrolytic polymer degradation experiments in PBS were performed using a TV-80-1 thermostat (Ryazan State Instrument-making Enterprise, Ryazan, Russian Federation). A series of five 60 × 10 × 1 mm rectangular samples of (co)polymers or composites prepared as

described in Section 2.5 were placed to PBS buffer solution (50 mL). At predetermined time periods, the samples were removed, dried using water-absorbing tissues, weighted, subjected to mechanical testing and analyzed using <sup>1</sup>H NMR spectroscopy and SEC.

## 3. Results and discussions

### 3.1. Preparation of pCap

In our previous study [40] we showed that micro-sized CAp species with different morphologies can be obtained hydrothermally when using Na<sub>2</sub>[EDTA] for dissolution of CaCO<sub>3</sub>. The shape and size of CAp crystallites, as well as CO<sub>3</sub><sup>2-</sup> content in the resulting CAp, are determined by pH of the reaction media, reaction time, temperature, nature and concentration of other reaction components (Na<sub>2</sub>HPO<sub>4</sub> or K(Na)H<sub>2</sub>PO<sub>4</sub>, Na<sub>2</sub>CO<sub>3</sub> or NaHCO<sub>3</sub>). During scaling and optimization of the process [41] we found that only two types of CAp can be obtained with a sufficiently high degree of reproducibility: hexagonal crystallites with ~1:1 aspect ratios (hCap), and plate-like crystallites (pCap). In this study, we also investigated compatibility of hCap and pCap with PLLA and found that the use of pCap provides better mechanical characteristics of the composites. We proposed that Ca<sup>2+</sup>-enriched surface in pCap [69] increases its affinity for polyesters. For this reason, pCap was selected as a filler in the present study.

The synthesis of pCap was conducted with minor changes in comparison with a published method [41] (see Section 2.4). The difference was that the heating to the reaction temperature was gradual, and the growth of pCap crystallites started from higher number of seeds. As a result, highly homogeneous sample without visible pCap splices was obtained (Fig. 1). X-ray diffraction studies confirmed B-type identity of pCap (the crystal cell parameters  $a = 9.429 \text{ \AA}$ ,  $c = 6.917 \text{ \AA}$ , see XRD pattern in Section S1 in the Appendix A), TGA and FT-IR data showed moderate incorporation of CO<sub>3</sub><sup>2-</sup> anions (4.1 and 4.8 wt.%, respectively). The Na/Ca ratio, estimated by SEM-EDX, was 0.09. These data illustrates good reproducibility of the method of the synthesis of pCap.

### 3.2. Synthesis, properties and molding of PLGAs and polymer composites

#### 3.2.1. Synthesis of PLGAs

In the present work, we first studied copolymerization of *L*-LA with *L*-MeGL, the experiment on copolymerization of *L*-LA with GL was conducted for comparison. Before polymerization experiments, the enantiomeric purity of *L*-LA and *L*-MeGL was estimated by optical rotation measurements. For *L*-LA [ $\alpha$ ]<sub>D</sub> was -295.7° (1.0 g·dL<sup>-1</sup>, toluene, 25 °C),

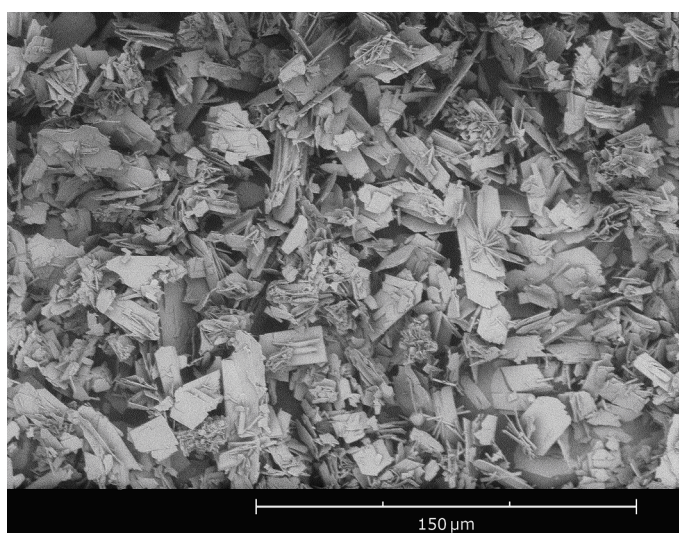


Fig. 1. SEM image of the pCap.

which complies with the reference data ( $[\alpha]_D = -296.0^\circ$ , toluene, 25 °C) [67]. The specific optical rotation  $[\alpha]_D$  of *L*-MeGL was  $-223.6^\circ$  (1.0 g·dL<sup>-1</sup>, CHCl<sub>3</sub>, 25 °C) which is noticeably higher by the absolute value than the reference data ( $[\alpha]_D = -220.5^\circ$  (1.0 g·dL<sup>-1</sup>, CHCl<sub>3</sub>, 0 °C) [62]).

Sn(Oct)<sub>2</sub> had been chosen as a polymerization catalyst, and stearyl alcohol was selected as an initiator. During copolymerization experiments, we obtained three samples: conventional *L*-PLGA 85/15 (the product of copolymerization of *L*-LA and GL), *L*-PLMG 85/15 and *L*-PLMG 70/30 (the products of copolymerization of *L*-LA and *L*-MeGL taken in 85:15 and 70:30 molar ratios, respectively). Note that the *L*-PLMG 70/30 copolymer is close to PLGA 85/15 in the ratio of *L*-lactate (L) and glycolate (G) fragments. The characteristics of (co)polymers are presented in Table 1.

### 3.2.2. Microstructure of (co)polymers

Based on previously published data [70,71], the analysis of <sup>13</sup>C NMR spectrum of commercial PLLA used in our study (Fig. S8 in the Appendix A) allowed to estimate the content of *d*-lactate fragments D by the value of at least 4%. This estimation was based on comparative integration of the signals at 69.14 and 69.57 ppm. In seminal work on the analysis of PLA microstructure [72] the signal at 69.57 ppm was attributed to *iss* tetrads. The similar spectral view was observed previously for *L*-LA homopolymer obtained with the use of aryloxy-magnesium catalyst [73] (see Fig. S9 in the Appendix A). Characteristic signals at 169.58, 169.50, 169.40 and 169.36 ppm also indicate the presence of *d*-lactate fragments in PLLA, identical spectral pattern was observed previously (see, for example, [74]). The signal at 169.36 ppm can be attributed to *isis* pentad [71], which increase the D content in PLLA to ~5%.

In <sup>1</sup>H NMR spectra of PLGAs with high glycolate content characteristic broad singlet at  $\delta \sim 4.8$  ppm is observed, this signal corresponds to GGG fragments [75]. The analysis of <sup>1</sup>H NMR spectra of *L*-LA-enriched PLGAs is a lot more problematic [76]. This analysis is essentially complicated by the fact that the signals of G fragments represent characteristic heminal AB system when CH<sub>2</sub> fragment is adjacent to L unit (LGG, LGL, GGL etc.). Such multiplicity is clearly visible as a pair of characteristic doublets at  $\delta \sim 4.9$  and 4.6 ppm in the <sup>1</sup>H NMR spectrum of alternating *L*-MeGL homopolymers of the formula (LG)<sub>n</sub> [55,56,62,63,77,78]. The recent studies of repeating sequence PLGAs by Meyer and coll. [56,78,79] have greatly expanded the types of L-G sequences that can be identified by the analysis of <sup>1</sup>H NMR spectra in the area of the signals of >CH- and -CH<sub>2</sub>- fragments.

The areas of the signals of glycolate and lactate protons in <sup>1</sup>H NMR spectra of *L*-PLGA 85/15, *L*-PLMG 85/15 and *L*-PLMG 70/30 are presented in Fig. 2. The spectrum of *L*-PLGA 85/15 is similar to published previously for commercial PLGA 2012D (Purac, Netherlands) [80] and *L*-PLGA 85/15 obtained using Zr(acac)<sub>4</sub> catalyst [76]. In the field of -CH<sub>2</sub>- signals, this spectrum is very complex (Fig. 2A, left), though the signal of GGG fragment at 4.81 ppm is clearly observed (this attribution is also confirmed by HMBC spectrum of *L*-PLGA 85/15, see Section S2 in the Appendix A). The main peaks in the field of L signals (Fig. 2B, left) can be attributed to LLL fragments. Based on our <sup>1</sup>H NMR spectral data and previously published results [56,76,80], it can be concluded that *L*-PLGA 85/15 represents copolymer containing (*L*-LA)<sub>n</sub> fragments interspersed with the GG, GGGG and even longer (GG)<sub>n</sub> inserts. The <sup>13</sup>C

NMR spectral data confirm this conclusion (see below).

The microstructure of *L*-PLMG 85/15 is easy to determine: the view of the -CH<sub>2</sub>- signals in <sup>1</sup>H NMR spectrum of *L*-PLMG 85/15 (Fig. 2A, center) is very similar to the glycolate peaks in the spectrum of poly(LLG) obtained by Meyer and coll. using SAP approach [56]. The spectral view of the L signals (Fig. 2B, center) is similar to *L*-PLGA 85/15 (mainly LLL fragments). It may therefore be concluded that the macromolecules of *L*-PLMG 85/15 comprise L<sub>n</sub> sequences with single G insertions, which is also confirmed by <sup>13</sup>C NMR spectral data (see below).

<sup>1</sup>H NMR spectrum of *L*-PLMG 70/30 is more complex. In the field of -CH<sub>2</sub>- peaks we observed the single left component of AB system (a in Fig. 2A, right), whereas the view of the right component clearly reflected the presence of G fragments in different environments, and two minor doublets seemed close in their intensity. The main signal (b in Fig. 2A, right) can be attributed to LLGLL fragment (very similar to LLG sequence revealed by Meyer and coll. [56], the peaks at 4.63 and 4.59 ppm). Comparison of the <sup>1</sup>H NMR spectrum of *L*-PLMG 70/30 with the spectrum of poly(*L*-LG) [63] indicates the absence of regioerrors LLGGLL, and therefore remaining two doublets (c, d in Fig. 2A, right) can be attributed to previously unobserved LLGLGGLL sequence. Multiplication of the signals of >CH- fragments (Fig. 2B, right) confirms this assumption.

In <sup>13</sup>C NMR spectra of *L*-PLGAs the signals of >C=O fragments are sensitive to sequential changes and thus can provide macromolecular fine structures and important sequential information. Numerous publications describe and discuss the <sup>13</sup>C NMR spectra of random PLGAs, obtained by polycondensation of *L*-lactic acid and glycolic acid [81,82] or by copolymerization of *L*-LA and GL [76,83–86]. However, the assignment of the signals in early and later works are often contradictory, the data matching is complicated by the use of different deuterated solvents. In the present work, we decided to keep building on the results of the studies of random [81,84,85] and sequence-controlled [56,78,79] PLGAs in the analysis of <sup>13</sup>C NMR spectra of new copolymers.

What is certain is that the signals of lactate >C=O (169–170 ppm) and glycolate >C=O (166–167 ppm) do not overlap. In <sup>13</sup>C NMR spectrum of *L*-PLGA 85/15 (Fig. 3A) the leftmost >C=O (L) peak at 169.73 ppm corresponds to LLLL fragment, the peaks further to the right evidently corresponds to L fragments chemically bound to G units (LLG, LLG, GLL, GLL etc.), the similar spectral view was observed previously for *L*-PLGAs obtained by polycondensation of *L*-lactic and glycolic acids [81]. In [75,81,84,85], the leftmost signal of >C=O (G) was attributed to (G)<sub>n</sub>, the signals of G fragments chemically bound to L units were observed more to the right. HMBC spectrum of *L*-PLGA 85/15 (Fig. 3D) also revealed the presence of (G)<sub>n</sub> fragments. Note that this pattern was observed for PLGAs solutions in CDCl<sub>3</sub> (we also used this solvent in our studies), in DMSO-d<sub>6</sub> the (G)<sub>n</sub> peak shifted to the right, adding to the confusion.

<sup>13</sup>C NMR spectrum of *L*-PLMG 85/15 (Fig. 3B) contains the only signal of >C=O (G) at 166.64 ppm that can be attributed to LLGLL fragment. In <sup>13</sup>C NMR spectrum of *L*-PLMG 70/30 (Fig. 3C) in the >C=O (G) field we also observe the main signal at 166.64 ppm. Note that this signal was detected in <sup>13</sup>C NMR spectrum of *L*-PLGA 85/15 (Fig. 3A) as a trace peak. The broadened signal at 166.58 ppm in the spectrum of *L*-PLMG 70/30 apparently corresponds to LLGLGGLL sequence detected

Table 1

Characteristics of (co)polymers under study.

(Co)polymer	mol.% L in feed	mol.% G in feed	Yield of PLGA, %	Comon. conv., <sup>1)</sup> %/%	mol.% L in copolymer <sup>2)</sup>	mol.% G in copolymer <sup>2)</sup>	M <sub>n</sub> , kDa <sup>3)</sup>	D <sub>M</sub> <sup>3)</sup>
PLLA	–	–	–	–	100	–	107.0	2.02
<i>L</i> -PLGA 85/15	85.0	15.0	81	80.9/81.5	84.9	15.1	83.1	2.15
<i>L</i> -PLMG 85/15	92.5	7.5	88	88.4/83.3	92.9	7.1	72.3	2.33
<i>L</i> -PLMG 70/30	85.0	15.0	86	86.0/86.0	85.0	15.0	65.7	2.27

<sup>1)</sup> *L*-LA/GL or *L*-LA/*L*-MeGL.

<sup>2)</sup> Determined by <sup>1</sup>H NMR analysis of the copolymers.

<sup>3)</sup> SEC data.

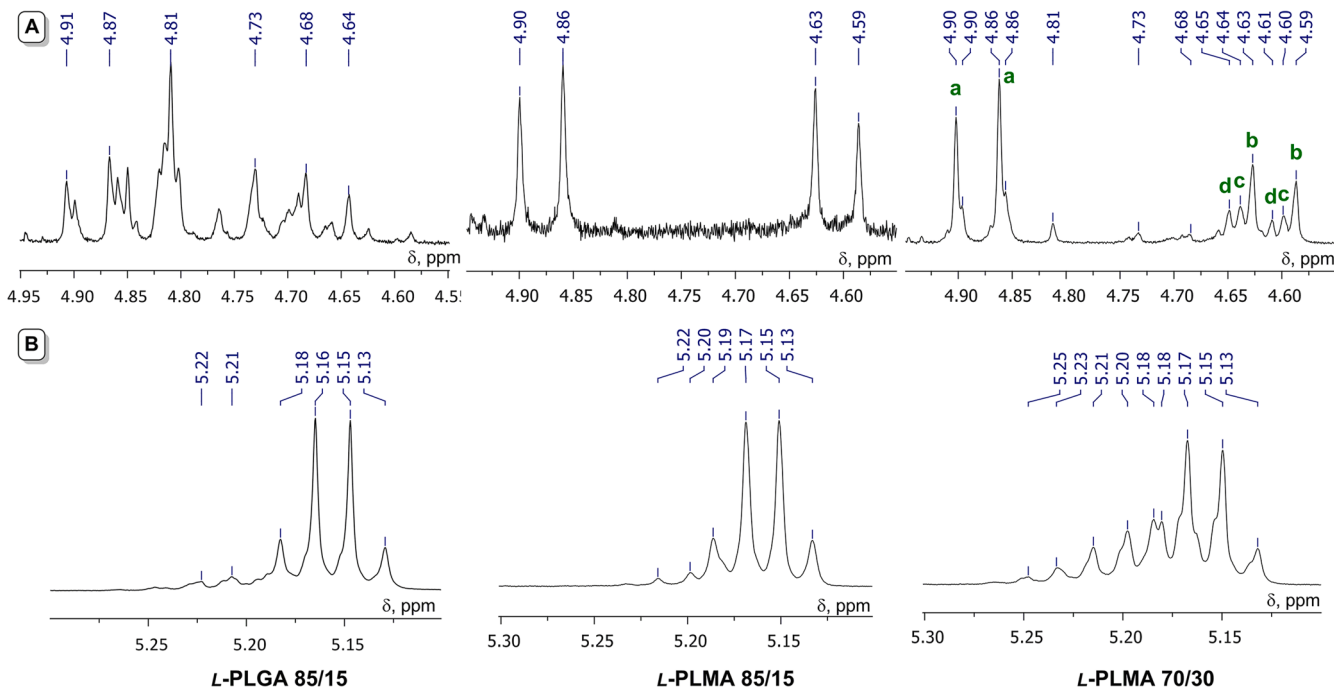


**Fig. 2.** The areas of the signals of glycolate  $-\text{CH}_2-$  (A) and lactate  $>\text{CH}-$  (B) fragments in  $^1\text{H}$  NMR spectra ( $\text{CDCl}_3$ ,  $25^\circ\text{C}$ , 400 MHz) of  $\iota$ -PLGA 85/15 (left),  $\iota$ -PLMG 85/15 (center) and  $\iota$ -PLMG 70/30 (right).

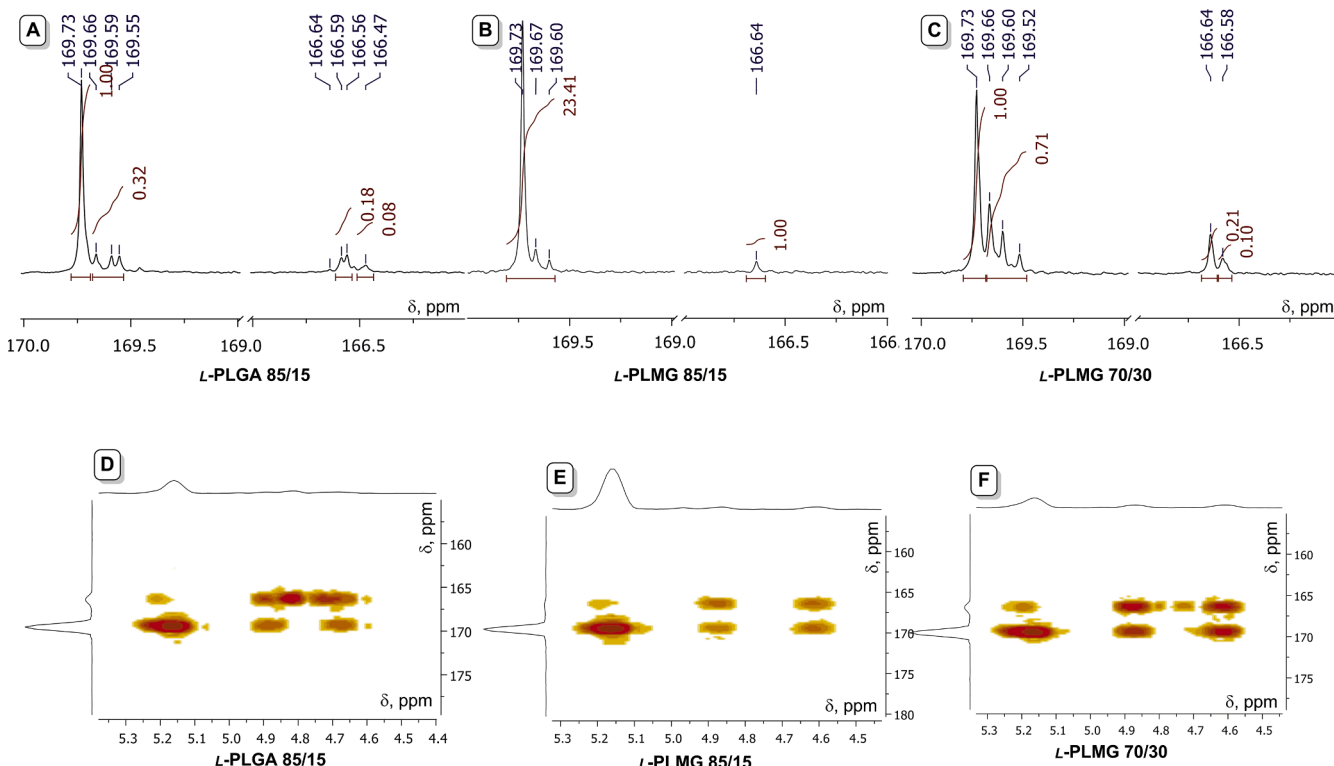


**Fig. 3.** The areas of the signals of lactate and glycolate  $>\text{C}=\text{O}$  fragments in  $^{13}\text{C}$  NMR spectra ( $\text{CDCl}_3$ , 25 °C, 101 MHz) of *l*-PLGA 85/15 (A), *l*-PLMG 85/15 (B) and *l*-PLMG 70/30 (C). The area of  $>\text{C}=\text{O}$  ( $^{13}\text{C}$ ) and  $>\text{CH}-/\text{CH}_2-$  ( $^1\text{H}$ ) correlations in HMBC spectra of *l*-PLGA 85/15 (D), *l*-PLMG 85/15 (E) and *l*-PLMG 70/30 (F).

using  $^1\text{H}$  NMR spectroscopy. In this case, the signal of lactate carbonyl at 169.52 ppm also corresponds to LLG<sub>n</sub>LGLL fragment. The signals of LGGL and other (G)<sub>n</sub>-containing fragments are not clearly visible in  $^{13}\text{C}$  NMR spectrum of *L*-PLMG 70/30, these fragments were observed in trace amounts in HMBC spectrum of *L*-PLMG 70/30 (Fig. 3F, full HMBC spectra of PLGAs are presented in Section S2 in the Appendix A).

Additional and crucial aspect of the analysis of  $^{13}\text{C}$  NMR spectra of synthesized PLGAs was the absence of peaks indicating epimerization of oligo(*L*-lactyl) fragments. As can be seen in Fig. S19 in the Appendix A, characteristic signals in carbonyl and methine regions, indicating the presence of stereoerrors in PLLA, are absent entirely in the spectra of all copolymers prepared.

Additional information on the (co)polymer microstructure and the presence of *L*-lactyl units can be obtained through the measurements of the optical rotation. For PLLA, the optical purity (content of *d*-lactyl fragments *D*) can be calculated by the Eq. (1) [87,88]

$$D(\%) = \frac{156 - \alpha_D^{20}(\text{PLLA})}{2 \times 156} \times 100\%, \quad (1)$$

where 156 is a specific optical rotation of enantiomerically pure PLLA in  $\text{CHCl}_3$  solution and  $\alpha_D^{20}$  is a specific optical rotation of the sample. For PLLA used in this work the measurements of the optical rotation yielded a  $\alpha_D^{20}$  value of  $-140.0^\circ$ ; and the calculated *D* value was  $\sim 5\%$ , which correlates with  $^{13}\text{C}$  NMR data.

The measurements of the optical rotation of PLGA solutions deserve special mention. The  $\alpha_D^{20}$  values ( $1.0 \text{ g}\cdot\text{dL}^{-1}$ ,  $\text{CHCl}_3$ ,  $25^\circ\text{C}$ ) for *L*-PLGA 85/15, *L*-PLMG 85/15 and *L*-PLMG 70/30 were  $-139.9^\circ$ ,  $-148.4^\circ$  and  $-147.5^\circ$ , respectively. In this way, *L*-PLGA 85/15 with lower content of *L*-lactyl units had  $\alpha_D^{20}$  value virtually equal to  $\alpha_D^{20}$  of commercial PLLA. Considering relatively high content of *d*-lactyl units in homopolymer this is quite understandable. It is also certain that  $\alpha_D^{20}$  value of *L*-PLMG 85/15 was higher in comparison with PLLA and conventional *L*-PLGA 85/15 considering higher *L*-lactyl content and the absence of *d*-lactyl units. Higher  $\alpha_D^{20}$  value observed in the case of *L*-PLMG 70/30 in comparison with *L*-PLGA 85/15 seems weird in view of equal *L*-lactyl content. However, based on the early basic work [89], we can propose that this disproportionate increase in the  $\alpha_D^{20}$  value can be attributed to higher statisticity of *L*-PLMG 70/30 in comparison with *L*-PLGA 85/15, resulting in shortening of the length of PLA fragments.

### 3.2.3. Thermal properties of (co)polymers

DSC studies have allowed us to determine the influence of the copolymer composition and microstructure on the thermal properties of polymers. Fig. 5 shows the curves obtained during the second sample heating scan. For all samples, the first noticeable effect was an inflection which indicates a glass transition of the polymer. The PLLA glass transition temperature  $T_g$  was the highest ( $59.2^\circ\text{C}$ ), for *L*-PLGA 85/15, *L*-PLMG 85/15 and *L*-PLMG 70/30  $T_g$  values were  $54.0$ ,  $55.5$  and  $55.0^\circ\text{C}$ , respectively. Such a small difference fully corresponds to the results of the studies of Meyer and coll. [56] who showed weak dependence of  $T_g$  on L/G ratio and sequence in PLGAs prepared using SAP approach. After the glass transition, a clear exothermic and endothermic effects were observed for PLLA and *L*-PLGA 85/15. The crystallization temperature ( $T_c$ ) of PLLA was  $123.0^\circ\text{C}$ ,  $T_c$  of *L*-PLGA 85/15 was  $127.9^\circ\text{C}$ . Noticeable was the difference in values of the melting temperatures  $T_m$ ,  $151.4^\circ\text{C}$  (PLLA) and  $161.7^\circ\text{C}$  (*L*-PLGA 85/15). The  $T_m = 158.0^\circ\text{C}$  was reported previously for *L*-PLGA 85/15 ( $M_n = 85.0 \text{ kDa}$ ,  $D_M = 1.9$ ) obtained with the use of  $\text{Zr}(\text{acac})_4$  catalyst, this copolymer had a  $T_g$  of  $58.2^\circ\text{C}$  [76]. These results confirms once again that the presence of *d*-lactyl units evenly distributed throughout the PLA chain have a great impact on the crystallization of the polymer. The crystal packing of enantiomerically pure PLLA occurs via formation of helical microstructural sequences [90, 91] and, as can be seen from the Fig. 4, the presence of *d*-lactyl units more severely affects the crystallization of the polymer vs the presence of oligo(G) inserts between enantiomerically pure relatively long PLA fragments. Apparently, in the case of *L*-PLGA 85/15 the absence of *d*-lactyl units allows long poly(*L*-LA) fragments to form crystalline segments with relatively high  $T_c$  and  $T_m$ .

DSC curves of both MeGL-based copolymers *L*-PLMG 85/15 and *L*-PLMG 70/30 did not contain melting and crystallization peaks (Fig. 4).

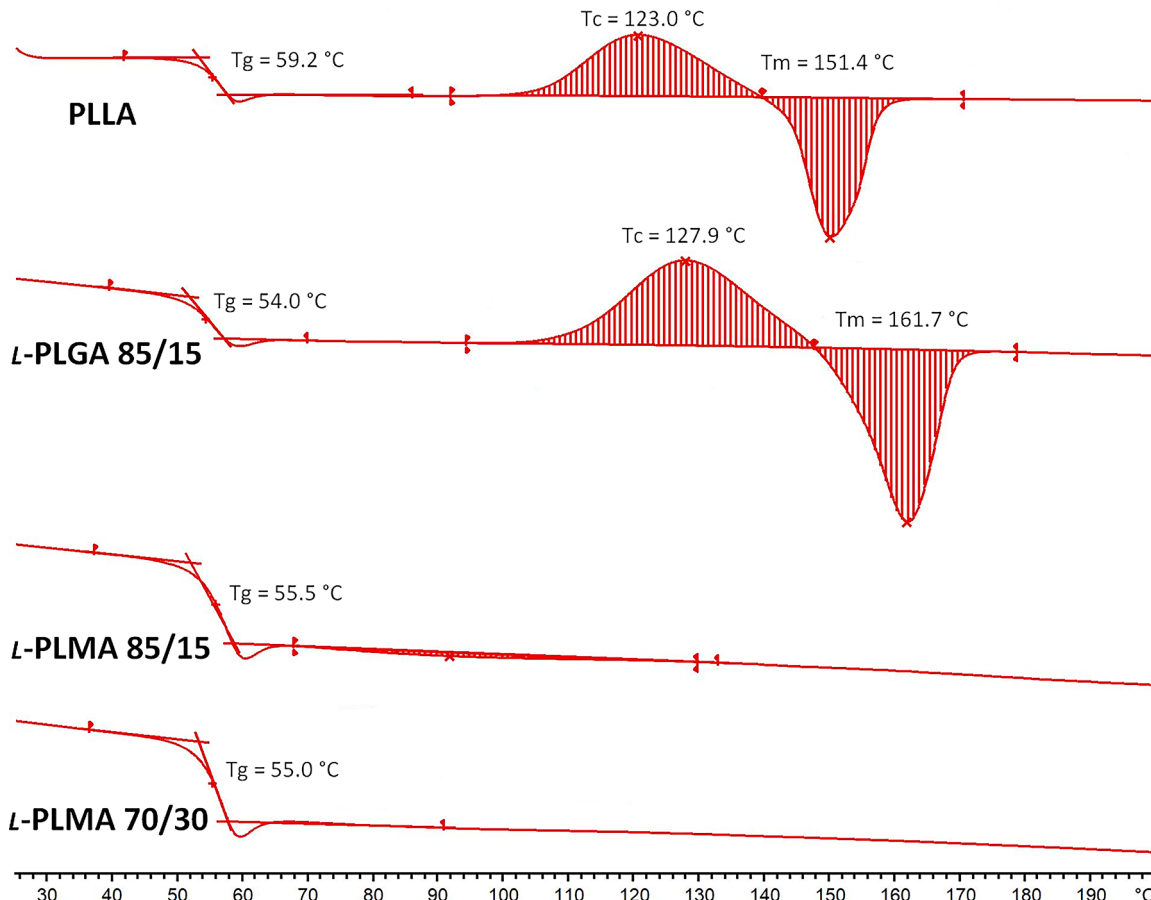


Fig. 4. The second heat scans of (co)polymers under study.

Apparently, *L*-MeGL based highly statistical copolymers having the average run numbers of the  $L_n$  fragments  $n = 12.3$  and  $5.7$ , respectively, form amorphous phases due to the absence of long  $L_n$  fragments provided by higher stochasticity of the coROP of *L*-MeGL in comparison with GL.

### 3.2.4. Preparation and characterization of copolymer and composite samples

The standard  $60 \times 10 \times 1$  mm rectangular plates were prepared from ground (co)polymers and from homogenized composite films containing 25 and 50 wt.% of pCap filler by injection molding at  $180^\circ\text{C}$  (copolymers) and  $185\text{--}190^\circ\text{C}$  (composites, see Section 2.5 for details). As can be seen in Fig. 5, homogenization and melt processing of the composites resulted in further grinding of pCap crystallites with a formation of well-dispersed particles of micron and submicron size. The chemical identity of the composites was confirmed by ATR FT-IR spectral studies (see Section S2.3 in the Appendix A).

Degradation of the polyester during melt processing greatly complicates making dense articles from PLLA and especially PLGA [92]. The effect of BMS on molecular weight and dispersity of PLA during melt mixing was detected previously in a number of works [11,41,93–95]. In the present study, we analyzed the changes in molecular weight characteristics of PLLA and copolymers during injection molding, the results are presented in Table 2. Among (co)polymers, PLLA demonstrated the highest thermal stability during molding at  $180^\circ\text{C}$ . For *L*-PLGA 85/15 more than twofold loss of  $M_n$  was detected with notable broadening of the molecular weight distribution. Suddenly, *L*-PLMG 70/30 turned out to be more stable in comparison with *L*-PLMG 85/15. The melt processing of the composites was conducted at  $185\text{--}190^\circ\text{C}$ , the presence of pCap in all cases increased the thermal degradation of (co)polymers during the melt processing (Table 2), however, the percentage of pCap evidently affected on the  $M_n$  of polymers: higher content of the filler lead to more pronounced degradation. This effect was more visible for PLLA and *L*-PLGA 85/15: so for example,  $M_n$  of PLLA, PLLA (25) and PLLA (50) (neat polymer and composites comprising 25 and 50 wt.% of the filler) were 83.3, 53.1 and 45.6 kDa.

The influence of the filler on the changes of  $M_n$  during melt processing can be explained by interaction of  $\text{Ca}^{2+}$ -enriched surface of pCap crystallites [69] with carbonyl oxygen atoms of the polyester chain. These interactions activates carbonyl groups and can facilitate chain scission by  $\text{OH}^-$  contained in pCap. However, the presence of  $\text{CO}_3^{2-}$  ions in pCap can mitigate degradation through binding of the acidic products, the positive impact of the presence of  $\text{CO}_3^{2-}$  ions in a filler on molecular weight of polyester matrix during injection molding was demonstrated previously [96].

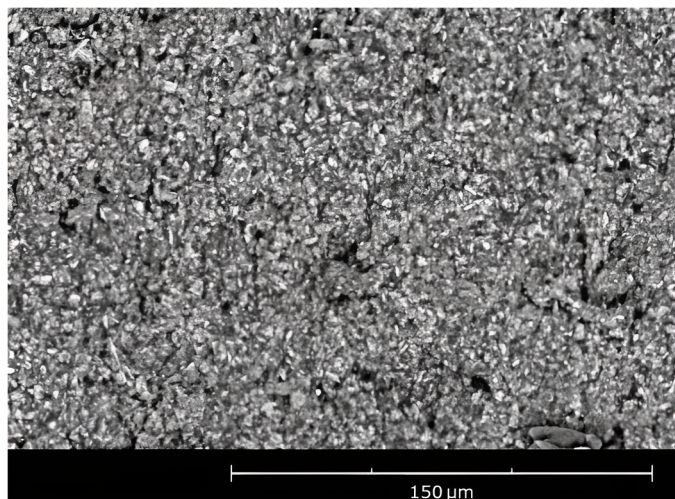


Fig. 5. SEM image of the surface of PLLA-50 composite.

**Table 2**

The changes in molecular weight characteristics of PLLA and PLGAs during injection molding of (co)polymers and (co)polymer composites with pCap (SEC data).

(Co) polymer	Before molding		After molding					
			Neat (co) polymer		Comp. 25% pCap		Comp. 50% pCap	
	$M_n$ , kDa	$D_M$	$M_n$ , kDa	$D_M$	$M_n$ , kDa	$D_M$	$M_n$ , kDa	$D_M$
PLLA	107.0	2.02	83.3	2.08	53.1	2.08	45.6	2.50
<i>L</i> -PLGA 85/15	83.1	2.15	33.5	2.91	28.4	2.82	19.4	2.28
<i>L</i> -PLMG 85/15	72.3	2.33	52.2	2.42	39.6	2.31	36.6	2.34
<i>L</i> -PLMG 70/30	65.7	2.27	53.2	2.31	41.7	2.14	39.5	2.22

### 3.3. Hydrolytic degradation of copolymer and composite samples

#### 3.3.1. Conducting experiments on hydrolytic degradation

Hydrolytic degradation experiments were performed for the series of 5 samples of (co)polymers and (co)polymer composites containing 25 and 50 wt.% of pCap filler. Each series of specimens was immersed in 50 mL of PBS buffer solution (pH 7.4). The specimens were extracted from the medium at specified intervals of time, the traces of the medium were removed from the sample surface using blotting paper. The specimens were weighed and subjected to mechanical testing. The samples for  $^1\text{H}$  NMR and DSC analyses were taken from undeformed parts of the specimens. The experiments were conducted during 43 days.

#### 3.3.2. The changes of the weight of the samples

As can be seen in Fig. 6, in the case of neat PLLA and *L*-PLMG 85/15 the weight of the sample does not increase. Apparently, this is due to high hydrophobicity of PLLA and *L*-PLMG 85/15 due to higher content of lactate units in comparison with other copolymers; in the latter case the presence of hydrophilic G fragments is offset by the fact that these fragments are isolated from each other by  $(L)_n$  fragments. In the case of *L*-PLGA 85/15 (Fig. 6B) we observed intense swelling up to 21.4% on day 43. The water uptake by the sample *L*-PLMG 70/30 (Fig. 6D) was less intensive (16.4% on day 43) in comparison with *L*-PLGA 85/15 apparently due to the absence of long hydrophilic  $(G)_n$  fragments in *L*-MeGL-based copolymer.

The composites containing 25% of pCap demonstrated different behavior depending on the nature of the matrix. The sample PLLA (25) gradually absorbed water, the average increase in the mass of the samples was 11.3% on day 43. All PLGA-based composites had demonstrated higher water absorption with maximum on day 28 for *L*-PLGA 85/15 (25), *L*-PLMG 85/15 (25) and *L*-PLMG 70/30 (25). The water uptake by composites containing 50% of filler was more diverse: the sample PLLA (50) strongly absorbed water within first 4 weeks, and the weight of the sample decreased on day 43. The water uptake by *L*-PLGA 85/15 (50), *L*-PLMG 85/15 (50) and *L*-PLMG 70/30 (50) was lower in comparison with the samples containing 25% of filler on day 43.

The changes of the weight of the samples during immersion may also be caused by (co)polymer degradation and chemical transformations of pCap. As can be seen in Section S2.3 in the Appendix A, FT-IR spectra of *L*-PLMG 70/30 and *L*-PLMG 70/30 (50) before and after hydrolysis are similar, which indicates the relative stability of pCap. FT-IR data are insufficient to determine the chemical transformations in polymer matrix, and the studies of molecular weight characteristics (SEC) and copolymer microstructure (NMR spectroscopy) were performed to identify these changes.

#### 3.3.3. The changes of molecular weight characteristics during hydrolytic degradation

For all (co)polymers under study, the  $M_n$  values gradually decreased

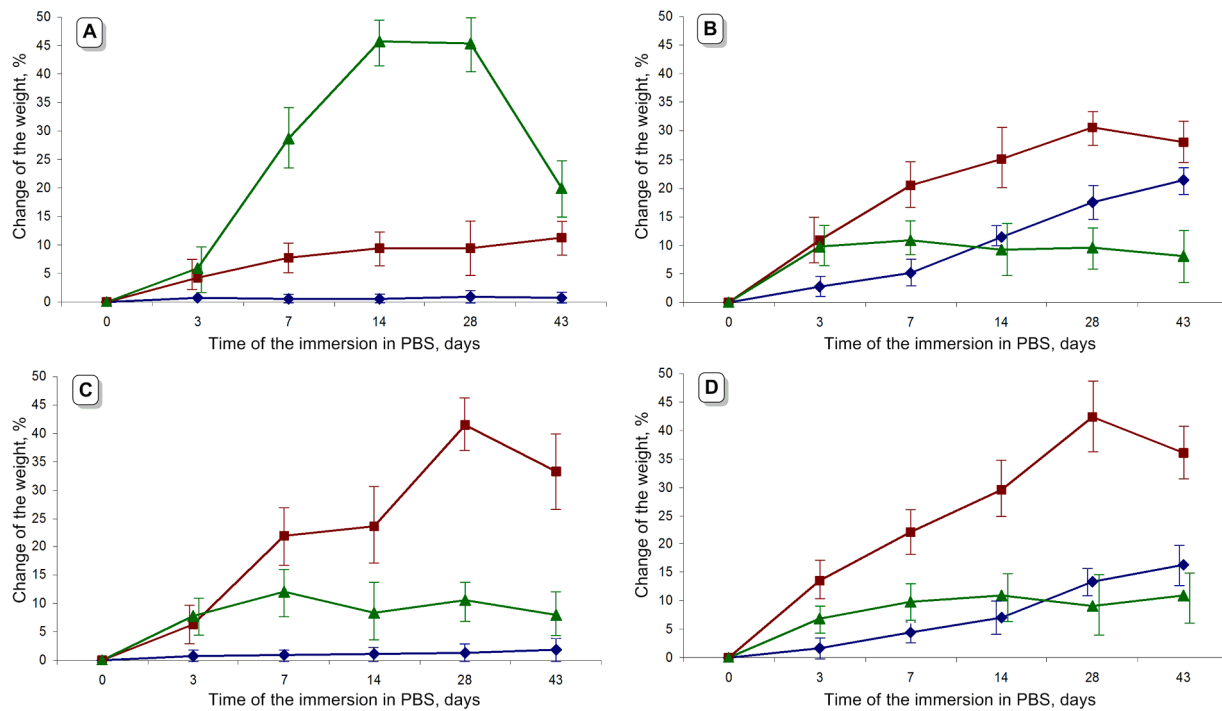


**Fig. 6.** The changes of the sample weight during immersion of the PLLA (A), *L*-PLGA 85/15 (B), *L*-PLMG 85/15 (C) and *L*-PLMG 70/30 (D) based specimens prepared from neat polymers (blue) and composites containing 25 wt.% (red) and 50 wt.% (green) of pCap.

during immersion in PBS (Fig. 7). Surprisingly, *L*-PLMG 85/15 was found to be the most hydrolytically stable among neat (co)polymers under study, after 43 days in PBS the  $M_n$  of *L*-PLMG 85/15 decreased by 35%. PLLA proved to be next in stability (decrease of  $M_n$  by 58% after 43 days of immersion). Predictably, *L*-PLGA 85/15 had the least hydrolytic stability: on day 43,  $M_n$  decreased by 89%. *L*-PLMG 70/30 with the same L/G ratio has lost 76% of  $M_n$  after 43 days. These results correspond to the

commonly accepted bulk erosion mechanism of hydrolytic degradation of PLA and PLGAs at neutral and acidic pH [97,98], (co)polymers with minimal water uptake were more stable. It is also essential to note that the hydrolysis of PLGAs is of the autocatalytic nature, higher local concentrations of acidic species enhance interior degradation and polymer erosion [99].

Starting the production of composites, we proposed that the presence

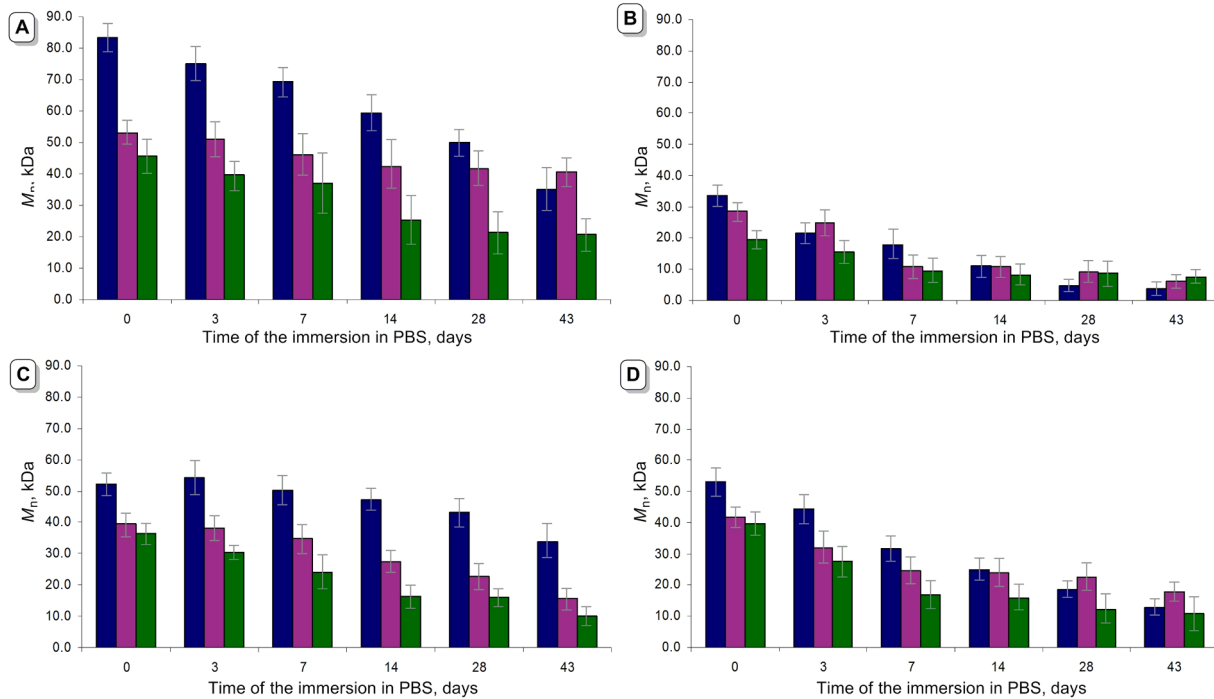


**Fig. 7.** The changes of the  $M_n$  of polymer matrixes during immersion of the PLLA (A), *L*-PLGA 85/15 (B), *L*-PLMG 85/15 (C) and *L*-PLMG 70/30 (D) based specimens prepared from neat polymers (blue) and composites containing 25 wt.% (red) and 50 wt.% (green) of pCap.

of basic pCap filler can slow down degradation due to the neutralization of the acidic degradation products by basic inorganic filler. For the most part, our assumption was proven correct. For PLLA (25), despite higher water uptake of the composite in comparison with PLLA, decrease of  $M_n$  amounted to 23% on day 43. However, in the case of PLLA (50) substantial decrease of  $M_n$  from 46 to 25 kDa was observed at the stage of intense swelling (first two weeks), at the end of which the  $M_n$  of the polymer matrix remained virtually unchanged, accounting for about ~21 kDa (Fig. 7A). In the case of *L*-PLGA 85/15 the stabilizing effect of pCap was more visible for *L*-PLGA 85/15 (50) (Fig. 7B). On the contrary, copolymers of *L*-MeGL degraded more slowly in composites containing 25 wt.% of the filler (Fig. 7C, D).

The molecular weight characteristics of neat (co)polymers and (co)polymer matrix in composites before and during degradation as well as selected SEC traces are presented in Section S2.2 in the Appendix A. Based on these data, in view of the presence or absence of low-MW degradation products in (co)polymer sample, it is possible to conclude that (co)polymer microstructure and the presence and content of the filler affect the degradation process.

In particular, relatively slow degradation of neat PLLA was accompanied by the formation of low-MW degradation products leached from the sample, the presence of minimal amount of low-MW oligomer was detected at day 14. For PLLA/pCap composites, low-MW oligomers were detected at initial stage (days 0 and 3), but unexpectedly high

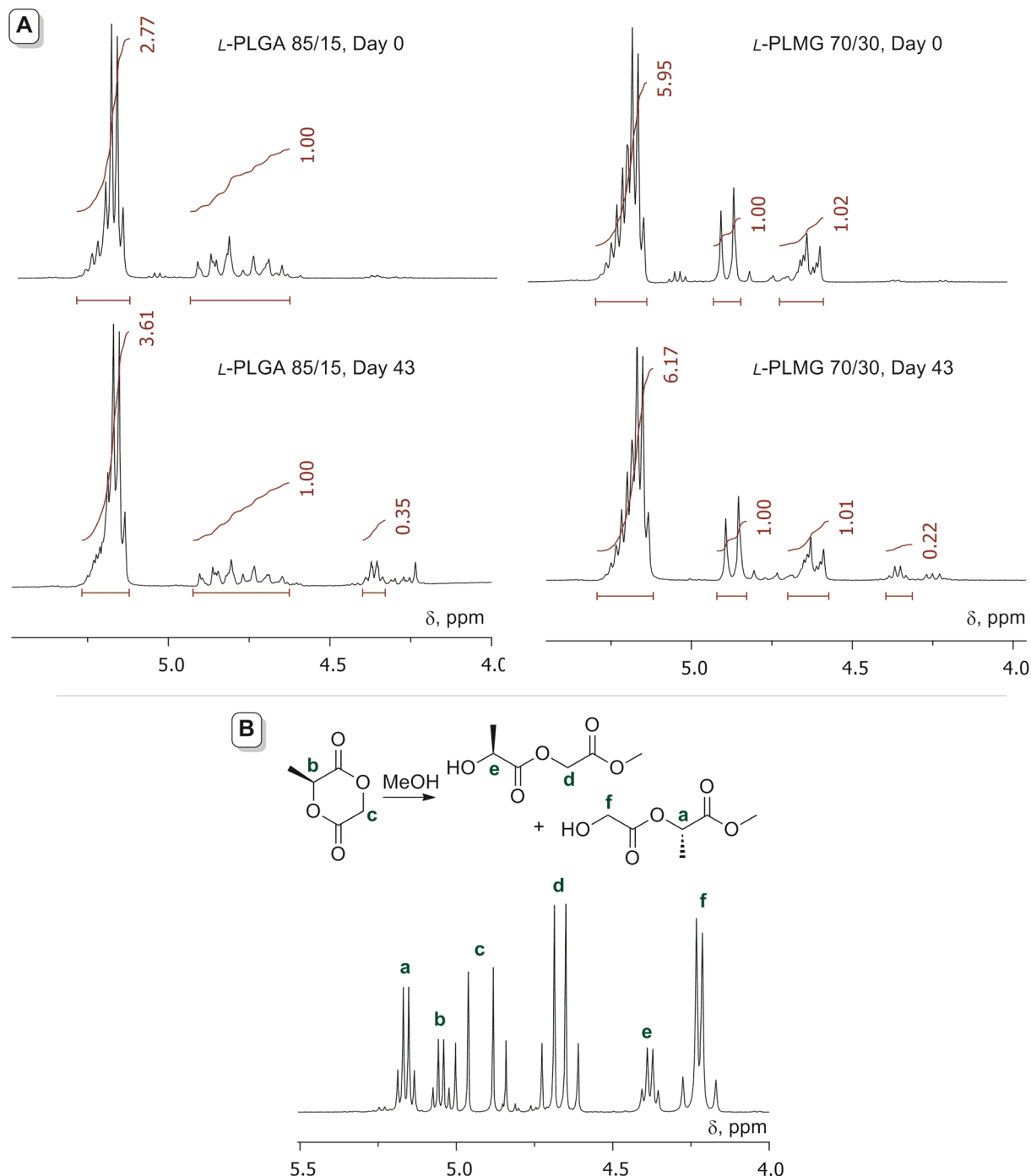


**Fig. 8.** (A) The signals of  $>\text{CH}-$  and  $-\text{CH}_2-$  fragments  $^1\text{H}$  NMR spectra ( $\text{CDCl}_3$ , 25 °C, 400 MHz) of *L*-PLGA 85/15 (left) and *L*-PLMG 70/30 (right) at day 0 (top) and day 43 (bottom). (B) The signals of  $>\text{CH}-$  and  $-\text{CH}_2-$  fragments in the reaction mixture formed during methanolysis of *L*-MeGL [61].

content of low-MW oligomers was observed for PLLA/pCap (50) sample in a week, on an active stage of swelling (see Fig. 6A). At later stages, these products were gradually washed out. Apparently, compatibility of pCap with relatively hydrophobic PLLA is limited and 50 wt.% concentration of the filler is excessive for this type of matrix. We propose that pronounced swelling is caused by further heterogenization, and low-MW oligomers remain bonded with hydrophobic PLLA matrix and wear off with time.

In the case of *L*-PLGA 85/15 and composites prepared with the use of this copolymer, low-MW degradation products were detected at the initial stages of hydrolysis. Later, low-MW degradation products were washed out, which may contribute to further hydrolysis in surrounding tissues with acidic response. On the contrary, low-MW degradation products were detected in all materials based on *L*-MeGL: they contained mainly lactate fragments and retained in the sample. In this way, the use of *L*-MeGL based copolymers significantly reduces the risks involved with the leaching of acidic low-MW degradation products and their impact on surrounding tissues. These observations are confirmed by the studies of L/G ratio in *L*-PLGA 85/15 and *L*-PLMG 70/30 remnants during degradation (see below).

### 3.3.4. The changes of the L/G ratio during hydrolytic degradation

The difference in microstructures of *L*-PLGA and *L*-PLMGs can not but affect the rate of hydrolytic degradation and the chemical composition of copolymer remnants. As can be seen in Fig. 8A, after 43 days of immersion in PBS the sample of *L*-PLGA 85/15 has lost a significant part of more reactive glycolate fragments whereas the sample of *L*-PLMG 70/30 has virtually retained the L/G ratio. This difference can be explained by vulnerability of hydrophilic and highly reactive G<sub>n</sub> segments in *L*-PLGA 85/15 to hydrolysis: the intensity of the peak at  $\delta = 4.81$  ppm, corresponding to GGGGG fragment, seems clearly lower after immersion in PBS. The similar effect was revealed previously when studying the degradation of PEG-*b*-PLGA copolymers [100].

For *L*-PLMG 70/30 the view of the area of the signals of glycolate protons remained virtually unchanged. The difference in the spectra of *L*-PLGA 85/15 and *L*-PLMG 70/30 before and after hydrolysis is also

manifested in the appearance of additional signal, quadruplet at  $\delta = 4.36$  ppm, that corresponds to -CHMeOH fragment of the product of hydrolysis. This attribution was made based on our previous studies [61] that revealed the signal of similar fragment during the experiment on methanolysis of *L*-MeGL (Fig. 8B), the appearance of -CHMeOH fragment is also in line with the results of the studies of controlled surface hydrolysis of PLGA that revealed the formation of the products containing -CHMeOH and -CH<sub>2</sub>COOH fragments [101].

### 3.4. Mechanical properties of copolymer and composite samples

The bending tests were conducted using the wet samples immediately after removal of the surface water. Every test was performed with a series of five  $60 \times 10 \times 1$  mm rectangular samples, the changes of the values of flexural moduli  $E_f$  are presented in Fig. 9. In earlier studies of PLLA and PLLA-based composites the positive impact of BMS content on  $E_f$  value had been demonstrated [11,102–104]. In our flexural tests, a twofold increase in  $E_f$  value was detected for PLLA (50) relative to PLLA (6.0 vs 3.2 GPa). The flexural strengths  $\sigma_f$  of the composites decreased with an increase of pCap content (100 MPa for PLLA, 71 and 48 MPa for PLLA (25) and PLLA (50), respectively, Fig. 10A). A similar pattern was observed for PLGAs and composites therefrom. Note that *L*-PLMG 85/15 (50) and *L*-PLMG 70/30 (50) initially demonstrated higher  $E_f$  values (8.4 and 8.7 GPa, respectively) in comparison with PLLA (6.0 GPa) and *L*-PLGA 85/15 (5.7 GPa).

Except PLLA, hydrolytic degradation resulted in sharp deterioration of the mechanical characteristics of (co)polymers and composites therefrom. In the case of PLLA (50) (Fig. 9A), the changes of the  $E_f$  values correlated with the swelling curve of this composite (Fig. 6A), its sealing on day 43 naturally led to strengthening. At the end of the 43-day experiment, PLLA (25) and PLLA (50) kept a fairly high  $E_f$  values (1.5 and 2.3 GPa, respectively), but the  $M_n$  values of the matrix remnants (Fig. 8A) had leveled off, and therefore these stable composites seem hardly suitable for bone substitution. In the case of PLGAs, the results were more complex but have revealed some prospective trends. *L*-PLGA 85/15 and *L*-PLGA 85/15-based composites unevenly lost their

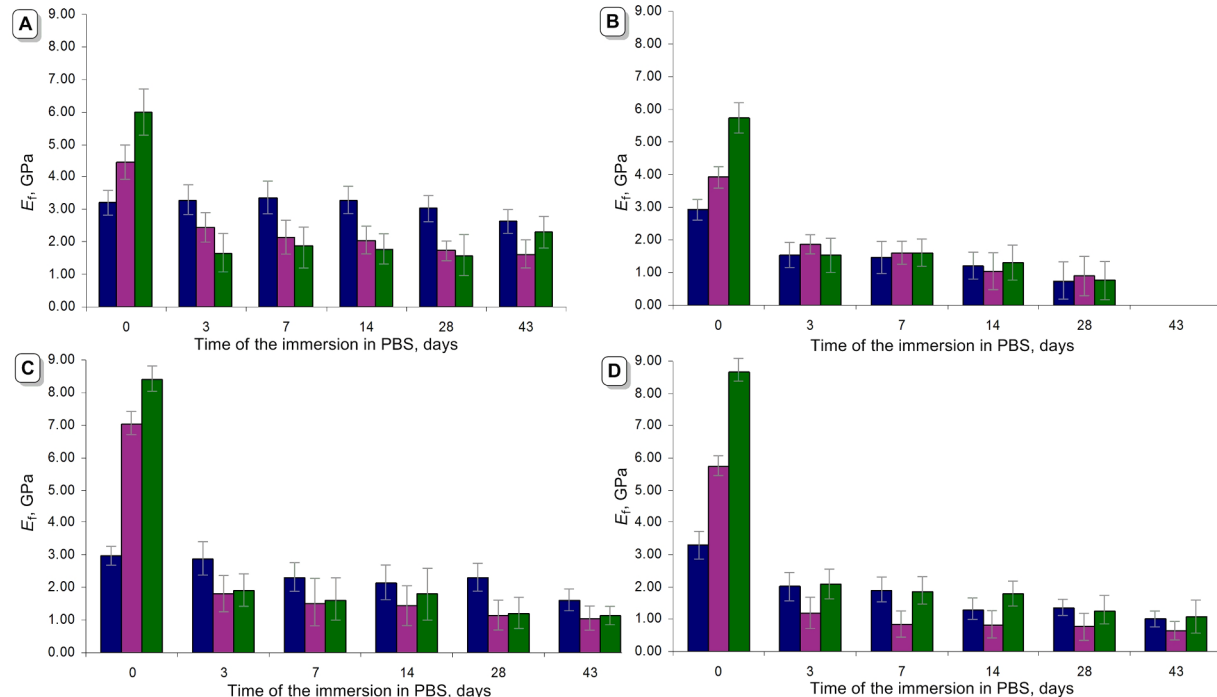


**Fig. 9.** The changes of the  $E_f$  during immersion of the PLLA (A), *L*-PLGA 85/15 (B), *L*-PLMG 85/15 (C) and *L*-PLMG 70/30 (D) based specimens prepared from neat polymers (blue) and composites containing 25 wt.% (red) and 50 wt.% (green) of pCap.

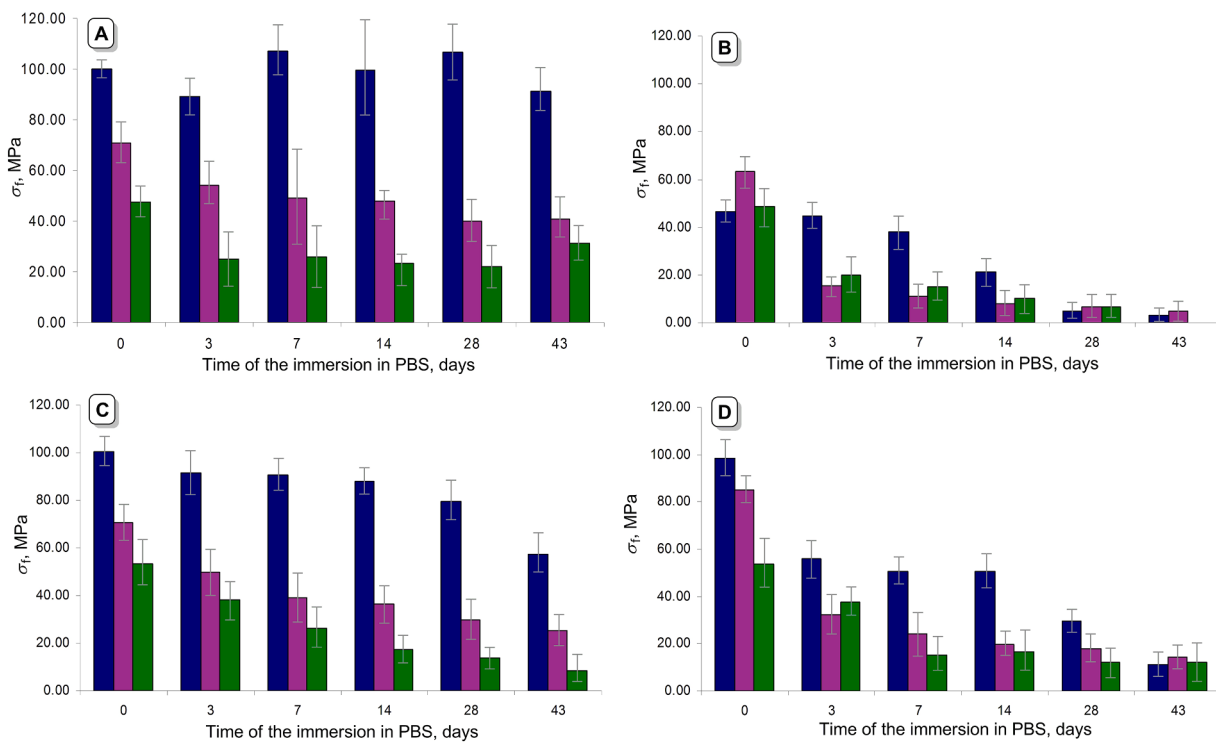


**Fig. 10.** The changes of the  $\sigma_f$  during immersion of the PLLA (A), L-PLGA 85/15 (B), L-PLMG 85/15 (C) and L-PLMG 70/30 (D) based specimens prepared from neat polymers (blue) and composites containing 25 wt.% (red) and 50 wt.% (green) of pCap.

mechanical strength to zero on the day 43, in which fragility of the samples had not allowed to conduct measurements. The similar pattern was observed for L-PLMG 85/15 and L-PLMG 70/30-based composites, however, these composites maintained their integrity in contrast with L-PLGA 85/15-based composites on day 43.

The changes of the flexural strength  $\sigma_f$  during hydrolytic degradation experiments (Fig. 10) also demonstrated the preference of L-MeGL-based PLGAs in comparison with conventional L-PLGA 85/15. By the results of our studies, the highest potential and prospects of L-MeGL in preparation of polymer matrixes for bone surgery and orthopedics seems obvious.

The interactions of pCap with (co)polymer matrix is an essential factor that influences the properties of the composites during hydrolytic degradation. 50 wt.% content of filler is excessively high for PLLA-based composite, but in the case of PLGA and PLMG-based composites the presence of more polar and less sterically hindered glycolate fragments provides higher compatibility of the filler and matrix. However, the formation of the acidic products during hydrolytic degradation cannot but affect the composite integrity which is particularly evident in the case of L-PLGA 85/15.

#### 4. Conclusions

For the first time, in this work we present new biodegradable materials of PLGA family – highly statistical copolymers of L-lactide and L-methylglycolide (L-MeGL), taken in molar ratio of 85:15 and 70:30. These copolymers, L-PLMG 85/15 and L-PLMG 70/30, were prepared by ring-opening copolymerization with the use of Sn(Oct)<sub>2</sub> catalyst; conventional L-PLGA 85/15 was synthesized by copolymerization of L-lactide with glycolide, taken in molar ratio of 85:15, and used as a reference material. New copolymers had microstructures, qualitatively distinct from conventional L-PLGA 85/15, as confirmed by NMR spectral studies. In particular, macromolecules of L-PLMG 85/15 comprised L<sub>n</sub> sequences with single G insertions, in L-PLMG 70/30 LLGLL and LLGLGLL fragments were detected. The absence of oligo(glycolate) fragments in L-PLMG has resulted in increase of hydrolytic stability of L-MeGL-based

copolymers in comparison with L-PLGA 85/15.

Using plate-like micro-sized carbonated apatite (pCap) as a filler, composites with 25 and 50 wt.% of pCap with poly(L-lactide), PLGA 85/15, L-PLMG 85/15 and L-PLMG 70/30 were prepared by injection molding. It was established that L-MeGL-based copolymers are more thermally stable in comparison with L-PLGA 85/15. Bending tests showed that composites, prepared from L-PLMG 85/15 and L-PLMG 70/30, are characterized by higher values of flexural moduli in comparison with PLLA- and PLGA 85/15-based composites. During immersion in phosphate buffer solution, all PLGA composites rapidly lose their strength, but L-MeGL-based matrixes provided higher hydrolytic stability of the composites.

The results of our preliminary studies showed that copolymers of L-lactide and L-MeGL are superior to PLGA 85/15 in thermal and hydrolytic stability. New L-MeGL-based copolymers appear to be capable of replacing conventional PLGAs in biomedical applications. Further optimization of the molding conditions, with the prospect of using compatibilizers to prevent thermal degradation of polymer matrix, could result in obtaining composite articles with significantly improved mechanical characteristics and tunable biodegradability. Intensive studies in this area are under way in our laboratory.

#### CRediT authorship contribution statement

**Alexander N. Tavorkin:** Software, Methodology, Investigation, Formal analysis, Data curation. **Egor A. Kretov:** Investigation, Data curation. **Maria P. Ryndyk:** Investigation. **Ilya E. Nifant'ev:** Writing – review & editing, Writing – original draft, Validation, Supervision, Resources, Project administration, Methodology, Investigation, Funding acquisition, Data curation, Conceptualization. **Andrey V. Shlyakhtin:** Software, Investigation. **Vladimir V. Bagrov:** Investigation. **Alexander A. Vinogradov:** Software, Investigation. **Pavel V. Ivchenko:** Writing – review & editing, Writing – original draft, Visualization, Validation, Software, Methodology, Formal analysis, Data curation, Conceptualization.

## Declaration of competing interest

The authors declare that they have no known competing financial interests or personal relationships that could have appeared to influence the work reported in this paper.

## Data availability

Data will be made available on request.

## Acknowledgement

The authors are thankful to the Russian Science Foundation, Grant No. 21–73–30010 for financial support.

## Supplementary materials

Supplementary material associated with this article can be found, in the online version, at [doi:10.1016/j.polymdegradstab.2024.110903](https://doi.org/10.1016/j.polymdegradstab.2024.110903).

## References

- [1] F.Y. Su, S. Pang, Y.T.T. Ling, P. Shyu, E. Novitskaya, K. Seo, S. Lambert, K. Zarate, O.A. Graeve, I. Jasiuk, J. McKittrick, Deproteinization of cortical bone: effects of different treatments, *Calcif. Tissue Int.* 103 (2018) 554–566, <https://doi.org/10.1007/s00223-018-0453-x>.
- [2] S. Pang, H.P. Schwarcz, I. Jasiuk, Interfacial bonding between mineral platelets in bone and its effect on mechanical properties of bone, *J. Mechani. Behav. Biomed. Mater.* 113 (2021) 104132, <https://doi.org/10.1016/j.jmbbm.2020.104132>.
- [3] N. Ramesh, S.C. Moratti, G.J. Dias, Hydroxyapatite–polymer biocomposites for bone regeneration: a review of current trends, *J. Biomed. Mater. Res. B Appl. Biomater.* 106 (2017) 2046–2057, <https://doi.org/10.1002/jbm.b.33950>.
- [4] S.M. George, C. Nayak, I. Singh, K. Balani, Multifunctional hydroxyapatite composites for orthopedic applications: a Review, *ACS Biomater. Sci. Eng.* 8 (2022) 3162–3186, <https://doi.org/10.1021/acsbiomaterials.2c00140>.
- [5] Z. Fu, J. Cui, B. Zhao, S.G. Shen, K. Lin, An overview of polyester/hydroxyapatite composites for bone tissue repairing, *J. Orthop. Transl.* 28 (2021) 118–130, <https://doi.org/10.1016/j.jot.2021.02.005>.
- [6] C.V. Rocha, V. Gonçalves, M.C. da Silva, M. Bañobre-López, J. Gallo, PLGA-based composites for various biomedical applications, *Int. J. Mol. Sci.* 23 (2022) 2034, <https://doi.org/10.3390/ijms23042034>.
- [7] P. Gentile, V. Chiono, I. Carmagnola, P.V. Hatton, An overview of poly(lactic-co-glycolic) acid (PLGA)-based biomaterials for bone tissue engineering, *Int. J. Mol. Sci.* 15 (2014) 3640–3659, <https://doi.org/10.3390/ijms15033640>.
- [8] S. Jin, X. Xia, J. Huang, C. Yuan, Y. Zuo, Y. Li, J. Li, Recent advances in PLGA-based biomaterials for bone tissue regeneration, *Acta Biomater.* 127 (2021) 56–79, <https://doi.org/10.1016/j.actbio.2021.03.067>.
- [9] Implants for surgery - calcium phosphates - Part 3: hydroxyapatite and  $\beta$ -tricalcium phosphate bone substitutes. 2017. Available online: [https://www.accessdata.fda.gov/scripts/cdrh/cfdocs/cfstandards/detail.cfm?standard\\_id=identification\\_no=35613](https://www.accessdata.fda.gov/scripts/cdrh/cfdocs/cfstandards/detail.cfm?standard_id=identification_no=35613) (accessed on 30 May 2024).
- [10] Z. Bal, T. Kaito, F. Korkusuz, H. Yoshikawa, Bone regeneration with hydroxyapatite-based biomaterials, *Emerg. Mater.* 3 (2020) 521–544, <https://doi.org/10.1007/s42247-019-00063-3>.
- [11] V.A. Demina, S.V. Krasheninnikov, A.I. Buzin, R.A. Kamyshinsky, N. V. Sadovskaya, E.N. Goncharov, N.A. Zhukova, M.V. Khvostov, A.V. Pavlova, T. G. Tolstikova, N.G. Sedush, S.N. Chvalun, Biodegradable poly( $\epsilon$ -lactide)/calcium phosphate composites with improved properties for orthopedics: effect of filler and polymer crystallinity, *Mater. Sci. Eng. C* 112 (2020) 110813, <https://doi.org/10.1016/j.msec.2020.110813>.
- [12] H. Shi, Z. Zhou, W. Li, Y. Fan, Z. Li, J. Wei, Hydroxyapatite based materials for bone tissue engineering: a brief and comprehensive introduction, *Crystals* 11 (2021) 149, <https://doi.org/10.3390/cryst11020149>.
- [13] A. Kuczumow, M. Gorzelak, J. Kosiński, A. Lasota, T. Blicharski, J. Gagala, J. Nowak, M. Jarzębski, M. Jabłonński, Hierarchy of bioapatites, *Int. J. Mol. Sci.* 23 (2022) 9537, <https://doi.org/10.3390/ijms23179537>.
- [14] K. Ishikawa, Carbonate apatite bone replacement: learn from the bone, *J. Ceramic Soc. Japan* 127 (2019) 595–601, <https://doi.org/10.2109/jcersj2.19042>.
- [15] M. Bohner, B. Le Gars Santoni, N. Döbelin,  $\beta$ -Tricalcium phosphate for bone substitution: synthesis and properties, *Acta Biomater.* 113 (2020) 23–41, <https://doi.org/10.1016/j.actbio.2020.06.022>.
- [16] I. Kovrlija, J. Locs, D. Loca, Octacalcium phosphate: innovative vehicle for the local biologically active substance delivery in bone regeneration, *Acta Biomater.* 135 (2021) 27–47, <https://doi.org/10.1016/j.actbio.2021.08.021>.
- [17] Y. Wu, L. Yang, L. Chen, M. Geng, Z. Xing, S. Chen, Y. Zeng, J. Zhou, K. Sun, X. Yang, B. Shen, Core-shell structured porous calcium phosphate bioceramic spheres for enhanced bone regeneration, *ACS Appl. Mater. Interf.* 14 (2022) 47491–47506, <https://doi.org/10.1021/acsami.2c15614>.
- [18] Y. Niu, T. Du, Y. Liu, Biomechanical characteristics and analysis approaches of bone and bone substitute materials, *J. Funct. Biomater.* 14 (2023) 212, <https://doi.org/10.3390/jfb14040212>.
- [19] K. Ishikawa, K. Hayashi, Carbonate apatite artificial bone, *Sci. Technol. Adv. Mater.* 22 (2021) 683–694, <https://doi.org/10.1080/14686996.2021.1947120>.
- [20] K. Deguchi, S. Nomura, A. Tsuchiya, I. Takahashi, K. Ishikawa, Effects of the carbonate content in carbonate apatite on bone replacement, *J. Tissue Eng. Regener. Med.* 16 (2022) 200–206, <https://doi.org/10.1002/term.3270>.
- [21] M. Safarzadeh, C.F. Chee, S. Ramesh, Effect of carbonate content on the in vitro bioactivity of carbonated hydroxyapatite, *Ceram. Int.* 48 (2022) 18174–18179, <https://doi.org/10.1016/j.ceramint.2022.03.076>.
- [22] M. Fujioka-Kobayashi, Y. Miyamoto, K. Ishikawa, T. Satomi, B. Schaller, Osteoclast behaviors on the surface of deproteinized bovine bone mineral and carbonate apatite substitutes in vitro, *J. Biomed. Mater. Res.* 110 (2022) 1524–1532, <https://doi.org/10.1002/jbm.a.37392>.
- [23] K. Hayashi, A. Tsuchiya, M. Shimabukuro, K. Ishikawa, Multiscale porous scaffolds constructed of carbonate apatite honeycomb granules for bone regeneration, *Mater. Des.* 215 (2022) 110468, <https://doi.org/10.1016/j.matdes.2022.110468>.
- [24] K. Hayashi, T. Yanagisawa, M. Shimabukuro, R. Kishida, K. Ishikawa, Granular honeycomb scaffolds composed of carbonate apatite for simultaneous intra- and inter-granular osteogenesis and angiogenesis, *Mater. Today Bio.* 14 (2022) 100247, <https://doi.org/10.1016/j.mtbiobio.2022.100247>.
- [25] K. Hayashi, R. Kishida, A. Tsuchiya, K. Ishikawa, Channel aperture characteristics of carbonate apatite honeycomb scaffolds affect ingrowths of bone and fibrous tissues in vertical bone augmentation, *Bioengineering* 9 (2022) 627, <https://doi.org/10.3390/bioengineering9110627>.
- [26] K. Shibahara, K. Hayashi, Y. Nakashima, K. Ishikawa, Reconstruction of load-bearing segmental bone defects using carbonate apatite honeycomb blocks, *ACS Mater. Au.* 3 (2023) 321–336, <https://doi.org/10.1021/acsmaterialsa.u3c00008>.
- [27] I. Atsuta, T. Mizokami, Y. Jinno, B. Ji, T. Xie, Y. Ayukawa, Synergistic effect of carbonate apatite and autogenous bone on, *Osteog. Mater.* 15 (2022) 8100, <https://doi.org/10.3390/ma15228100>.
- [28] D. Fadilah, A.H. Zuratal Ain, A. Nurazreena, Y. Badrul Hisham, Y. Sawibah, O. Jer Ping, M.Y. Loqman, M. Mariatti, In vivo efficacy of carbonate apatite based scaffold in a New Zealand white rabbit, *Mater. Today Proc.* 66 (2022) 2752–2755, <https://doi.org/10.1016/j.mtpr.2022.06.509>.
- [29] N. Fukuda, K. Kudoh, K. Akita, N. Takamaru, K. Ishikawa, Y. Miyamoto, Comparison of bioresorbable bone substitutes, carbonate apatite and  $\beta$ -tricalcium phosphate, for alveolar bone augmentation with simultaneous implant placement, *Oral Sci. Int.* 20 (2023) 221–228, <https://doi.org/10.1002/osi2.1170>.
- [30] R. Takahashi, I. Atsuta, I. Narimatsu, T. Yamaza, X. Zhang, Y. Egashira, K. Koyano, Y. Ayukawa, Evaluation of carbonate apatite as a bone substitute in rat extraction sockets from the perspective of mesenchymal stem cells, *Dent. Mater.* 42 (2023) 282–290, <https://doi.org/10.4012/dmj.2022-040>.
- [31] K. Kudoh, N. Fukuda, K. Akita, T. Kudoh, N. Takamaru, N. Kurio, K. Hayashi, K. Ishikawa, Y. Miyamoto, Reconstruction of rabbit mandibular bone defects using carbonate apatite honeycomb blocks with an interconnected porous structure, *J. Mater. Sci. Mater. Med.* 34 (2023) 2, <https://doi.org/10.1007/s10865-022-06710-2>.
- [32] W. Linhart, F. Peters, W. Lehmann, K. Schwarz, A.F. Schilling, M. Amling, J. M. Rueger, M. Epple, Biologically and chemically optimized composites of carbonated apatite and polyglycolide as bone substitution materials, *J. Biomed. Mater. Res.* 54 (2001) 162–171, [https://doi.org/10.1002/1097-4636\(200102\)54:2<162::AID-JBM2>3.0.CO;2-3](https://doi.org/10.1002/1097-4636(200102)54:2<162::AID-JBM2>3.0.CO;2-3).
- [33] M. Schardosim, J. Soulié, D. Poquillon, S. Cazalbou, B. Dupoyer, C. Tenailleau, C. Rey, R. Hübler, C. Combes, Freeze-casting for PLGA/carbonated apatite composite scaffolds: structure and properties, *Mater. Sci. Eng. C* 77 (2017) 731–738, <https://doi.org/10.1016/j.msec.2017.03.302>.
- [34] E. Garskaite, L. Alinauskas, M. Drienovsky, J. Krajkovic, R. Cicika, M. Palcut, L. Jonusauskas, M. Malinauskas, Z. Stankeviute, A. Kareiva, Fabrication of a composite of nanocrystalline carbonated hydroxyapatite (cHAP) with polyactic acid (PLA) and its surface topographical structuring with direct laser writing (DLW), *RSC Adv.* 6 (2016) 72733–72743, <https://doi.org/10.1039/c6ra11679e>.
- [35] B.I. Oladapo, I.A. Daniyani, O.M. Ikumapayi, O.B. Malachi, I.O. Malachi, Microanalysis of hybrid characterization of PLA/cHA polymer scaffolds for bone regeneration, *Polym. Test.* 83 (2020) 106341, <https://doi.org/10.1016/j.polymertesting.2020.106341>.
- [36] C. Zhang, K. Hayashi, K. Ishikawa, Osseointegration enhancement by controlling dispersion state of carbonate apatite in polylactic acid implant, *Coll. Surf. B Biointerf.* 232 (2023) 113588, <https://doi.org/10.1016/j.colsurfb.2023.113588>.
- [37] J.M. Delgado-López, M. Lafisco, I. Rodríguez, A. Tampieri, M. Prat, J. Gómez-Morales, Crystallization of bioinspired citrate-functionalized nanoapatite with tailored carbonate content, *Acta Biomater.* 8 (2012) 3491–3499, <https://doi.org/10.1016/j.actbio.2012.04.046>.
- [38] F. Ren, Y. Leng, Y. Ding, K. Wang, Hydrothermal growth of biomimetic carbonated apatite nanoparticles with tunable size, morphology and ultrastructure, *CrystEngComm* 15 (2013) 2137–2146, <https://doi.org/10.1039/c3ce2684e>.
- [39] J.M. Delgado-López, R. Frison, A. Cervellino, J. Gómez-Morales, A. Guagliardi, N. Masciocchi, Crystal size, morphology, and growth mechanism in bio-inspired apatite nanocrystals, *Adv. Funct. Mater.* 24 (2014) 1090–1099, <https://doi.org/10.1002/adfm.201302075>.
- [40] I.E. Nifant'ev, A. Tavorkin, S.A. Legkov, S.A. Korchagina, G.A. Shandryuk, E. A. Kretov, A.O. Dmitrienko, P.V. Ivchenko, Hydrothermal synthesis of perfectly

- shaped micro- and nanosized carbonated apatite, *Inorg. Chem. Front.* 8 (2021) 4976–4989, <https://doi.org/10.1039/diqj01094h>.
- [41] I. Nifant'ev, A. Tavtorkin, P. Komarov, E. Kretov, S. Korchagina, M. Chinova, D. Gavrilov, P. Ivchenko, Dispersant and protective roles of amphiphilic poly(ethylene phosphate) block copolymers in polyester/bone mineral composites, *Int. J. Mol. Sci.* 24 (2023) 11175, <https://doi.org/10.3390/ijms24131175>.
- [42] I.E. Nifant'ev, A.N. Tavtorkin, M.P. Ryndyk, D.E. Gavrilov, Y.S. Lukina, L. Bonyshhev-Abramov, N.B. Serejnikova, D.V. Smolentsev, P. Ivchenko, Crystalline micro-sized carbonated apatites: chemical anisotropy of the crystallite surfaces, biocompatibility, osteoconductivity, and osteoinductive effect enhanced by poly(ethylene phosphoric acid), *ACS Appl. Bio Mater.* 6 (2023) 5067–5077, <https://doi.org/10.1021/acsabm.3c00753>.
- [43] S. Farah, D.G. Anderson, R. Langer, Physical and mechanical properties of PLA, and their functions in widespread applications – a comprehensive review, *Adv. Drug Deliv. Rev.* 107 (2016) 367–392, <https://doi.org/10.1016/j.addr.2016.06.012>.
- [44] S. Liu, S. Qin, M. He, D. Zhou, Q. Qin, H. Wang, Current applications of poly(lactic acid) composites in tissue engineering and drug delivery, *Compos. B Eng.* 199 (2020) 108238, <https://doi.org/10.1016/j.compositesb.2020.108238>.
- [45] H.K. Makadia, S.J. Siegel, Poly-lactic-co-glycolic acid (PLGA) as biodegradable controlled drug delivery carrier, *Polymers* 3 (2011) 1377–1397, <https://doi.org/10.3390/polym3031377>.
- [46] I.E. Nifant'ev, A.N. Tavtorkin, A.V. Shlyakhtin, P.V. Ivchenko, Chemical features of the synthesis, degradation, molding and performance of poly(lactic-co-glycolic) acid (PLGA) and PLGA-based articles 215 (2024) 113250, <https://doi.org/10.1016/j.europolymj.2024.113250>.
- [47] A. Roointan, S. Kianpour, F. Memari, M. Gandomani, S.M.G. Hayat, S. Mohammadi-Samanii, Poly(lactic-co-glycolic acid): the most ardent and flexible candidate in biomedicine! *Int. J. Polym. Mater. Polym. Biomater.* 67 (2018) 1028–1049, <https://doi.org/10.1080/00914037.2017.1405350>.
- [48] D. Zhao, T. Zhu, J. Li, L. Cui, Z. Zhang, X. Zhuang, J. Ding, Poly(lactic-co-glycolic acid)-based composite bone-substitute materials, *Bioact. Mater.* 6 (2021) 346–360, <https://doi.org/10.1016/j.bioactmat.2020.08.016>.
- [49] X. Sun, C. Xu, G. Wu, Q. Ye, C. Wang, Poly(Lactic-co-Glycolic Acid): applications and future prospects for periodontal tissue regeneration, *Polymers* 9 (2017) 189, <https://doi.org/10.3390/polym9060189>.
- [50] Y. Matsuda, M. Karino, T. Okui, T. Kanno, Complications of Poly-L-Lactic acid and polyglycolic acid (PLLA/PGA) osteosynthesis systems for maxillofacial surgery: a retrospective clinical investigation, *Polymers* 13 (2021) 889, <https://doi.org/10.3390/polym13060889>.
- [51] R. Song, M. Murphy, C. Li, K. Ting, C. Soo, Z. Zheng, Current development of biodegradable polymeric materials for biomedical applications, *Drug Des. Dev. Ther.* 12 (2018) 3117–3145, <https://doi.org/10.2147/DDDT.S165440>.
- [52] I.E. Nifant'ev, A.V. Shlyakhtin, V.V. Bagrov, P.D. Komarov, A.N. Tavtorkin, M. E. Minyaev, P.V. Ivchenko, Efficient synthetic approach to copolymers of glycolic and lactic acids for biomedical applications, *Mendeleev Commun* 28 (2018) 412–414, <https://doi.org/10.1016/j.mencom.2018.07.024>.
- [53] D.W. Grijpma, A.J. Nijenhuis, A.J. Pennings, Synthesis and hydrolytic degradation behaviour of high-molecular-weight L-lactide and glycolide copolymers, *Polymer* 31 (1990) 2201–2206, [https://doi.org/10.1016/0032-3861\(90\)90096-H](https://doi.org/10.1016/0032-3861(90)90096-H).
- [54] J. Li, P. Nemes, J. Guo, Mapping intermediate degradation products of poly(lactic-co-glycolic acid) in vitro, *J. Biomed. Mater. Res.* 106 (2018) 1129–1137, <https://doi.org/10.1002/jbm.b.33920>.
- [55] R.M. Stayhich, T.Y. Meyer, Preparation and microstructural analysis of poly(lactic-alt-glycolic acid), *J. Polym. Sci. A Polym. Chem.* 46 (2008) 4704–4711, <https://doi.org/10.1002/pola.22801>.
- [56] R.M. Stayhich, T.Y. Meyer, New insights into poly(lactic-co-glycolic acid) microstructure: using repeating sequence copolymers to decipher complex NMR and thermal behavior, *J. Am. Chem. Soc.* 132 (2010) 10920–10934, <https://doi.org/10.1021/ja102670n>.
- [57] C.M. Dong, K.-Y. Qiu, Z.-W. Gu, X.-D. Feng, Measurement of monomer reactivity ratios of D,L-D-Lethylglycolide with glycolide or D,L-DaLtide, *Chin. Chem. Lett.* 11 (2000) 815–818.
- [58] Z.-R. Shen, J.-H. Zhu, Z. Ma, Synthesis and characterization of poly(DL-lactic acid/glycolic acid), *Makromol. Chem. Rapid Commun.* 14 (1993) 457–460, <https://doi.org/10.1002/marc.1993.030140715>.
- [59] C.-M. Dong, K.-Y. Qiu, Z.-W. Gu, X.-D. Feng, Synthesis of poly(D,L-lactic acid-alt-glycolic acid) from D,L-D-Lethylglycolide, *J. Polym. Sci. A Polym. Chem.* 38 (2000) 4179–4184, [https://doi.org/10.1002/1099-0518\(20001201\)38:23<4179::AID-POLA20>3.0.CO;2-5](https://doi.org/10.1002/1099-0518(20001201)38:23<4179::AID-POLA20>3.0.CO;2-5).
- [60] C.-M. Dong, K.-Y. Qiu, Z.-W. Gu, X.-D. Feng, Living polymerization of D,L-D-Lethylglycolide initiated with bimetallic (Al/Zn)  $\mu$ -oxo alkoxide and copolymers thereof, *J. Polym. Sci. A Polym. Chem.* 39 (2001) 357–367, [https://doi.org/10.1002/1099-0518\(20010201\)39:3<357::AID-POLA1003>3.0.CO;2-0](https://doi.org/10.1002/1099-0518(20010201)39:3<357::AID-POLA1003>3.0.CO;2-0).
- [61] I.E. Nifant'ev, A.V. Shlyakhtin, V.V. Bagrov, A.N. Tavtorkin, P.D. Komarov, A. V. Churakov, P.V. Ivchenko, Substituted glycolides from natural sources: preparation, alcoholysis and polymerization, *Polym. Chem.* 11 (2020) 6890–6902, <https://doi.org/10.1039/d0py01297a>.
- [62] K. Takojima, H. Makino, T. Saito, T. Yamamoto, K. Tajima, T. Isono, T. Satoh, An organocatalytic ring-opening polymerization approach to highly alternating copolymers of lactic acid and glycolic acid, *Polym. Chem.* 11 (2020) 6365–6373, <https://doi.org/10.1039/d0py01082k>.
- [63] Y. Lu, J.H. Swisher, T.Y. Meyer, G.W. Coates, Chirality-directed regioselectivity: an approach for the synthesis of alternating poly(Lactic-co-Glycolic Acid), *J. Am. Chem. Soc.* 143 (2021) 4119–4124, <https://doi.org/10.1021/jacs.1c00248>.
- [64] Y. Rusconi, M.C. D'Alterio, C. De Rosa, Y. Lu, S.M. Severson, G.W. Coates, G. Talarico, Mechanism of alternating poly(lactic-co-glycolic acid) formation by polymerization of (s)- and (r)-3-methyl glycolide using an enantiopure aluminum complex, *ACS Catal.* 14 (2024) 318–323, <https://doi.org/10.1021/acscatal.3c04955>.
- [65] E. Altay, Y.-J. Jang, X.Q.i Kua, M.A. Hillmyer, Synthesis, microstructure, and properties of high-molar-mass polyglycolide copolymers with isolated methyl defects, *Biomacromolecules* 22 (2021) 2532–2543, <https://doi.org/10.1021/acs.biomac.1c00269>.
- [66] S. Ji, X. Zhang, M. Han, The guiding assemble method and block copolymer template of a kind of block copolymer, manufacturing cycle nanostructure, Patent CN108546328 (2018). <https://patents.google.com/patent/CN108546328A/en>.
- [67] L. Feng, X. Bian, Z. Chen, S. Xiang, Y. Liu, B. Sun, G. Li, X. Chen, Determination of D-lactide content in lactide stereoisomeric mixture using gas chromatography-polarimetry, *Talanta* 164 (2017) 268–274, <https://doi.org/10.1016/j.talanta.2016.11.038>.
- [68] B. Lozhkin, A. Shlyakhtin, V. Bagrov, P. Ivchenko, I. Nifant'ev, Effective stereoselective approach to substituted 1,4-dioxan-2,5-diones as prospective substrates for ring-opening polymerization, *Mendeleev. Commun* 28 (2018) 61–63, <https://doi.org/10.1016/j.mencom.2018.01.020>.
- [69] L. Pastero, M. Bruno, D. Aquilano, Habit change of monoclinic hydroxyapatite crystals growing from aqueous solution in the presence of citrate ions: the role of 2D epitaxy, *Crystals* 8 (2018) 308, <https://doi.org/10.3390/crys8080308>.
- [70] M.T. Zell, B.E. Padden, A.J. Paterick, K.A.M. Thakur, R.T. Kean, M.A. Hillmyer, E. J. Munson, Unambiguous determination of the  $^{13}\text{C}$  and  $^1\text{H}$  NMR stereosequence assignments of polylactide using high-resolution solution nmr spectroscopy, *Macromolecules* 35 (2002) 7700–7707, <https://doi.org/10.1021/ma0204148>.
- [71] P. Zhao, Q.-F. Wang, Q. Zhong, N.-W. Zhang, J. Ren, Microstructure and mechanism study of polylactide obtained by the copolymerization of L-lactide and D,L-DaLtide, *J. Appl. Polym. Sci.* 115 (2010) 2955–2961, <https://doi.org/10.1002/app.31387>.
- [72] M. Bero, J. Kasperczyk, Z.J. Jedlinski, Coordination polymerization of lactides, 1. Structure determination of obtained polymers, *Makromol. Chem.* 191 (1990) 2287–2296, <https://doi.org/10.1002/macp.1990.021911007>.
- [73] I. Nifant'ev, P. Komarov, V. Ovchinnikova, A. Kiselev, M. Minyaev, P. Ivchenko, Comparative experimental and theoretical study of Mg, Al and Zn aryloxy complexes in copolymerization of cyclic esters: the role of the metal coordination in formation of random copolymers, *Polymers* 12 (2020) 2273, <https://doi.org/10.3390/polym12102273>.
- [74] G.-X. Chen, H.-S. Kim, E.-S. Kim, J.-S. Yoon, Synthesis of high-molecular-weight poly(L-lactic acid) through the direct condensation polymerization of L-lactic acid in bulk state, *Eur. Polym. J.* 42 (2006) 468–472, <https://doi.org/10.1016/j.europolymj.2005.07.022>.
- [75] J. Sun, J. Walker, M. Beck-Broichsitter, S.P. Schwendeman, Characterization of commercial PLGAs by NMR spectroscopy, *Drug Deliv. Transl. Res.* 12 (2022) 720–729, <https://doi.org/10.1002/s13346-021-01023-3>.
- [76] P. Dobrzynski, J. Kasperczyk, H. Janecek, M. Bero, Synthesis of biodegradable copolymers with the use of low toxic zirconium compounds. 1. copolymerization of glycolide with L-Lactide initiated by  $\text{Zr}(\text{Acac})_4$ , *Macromolecules* 34 (2001) 5090–5098, <https://doi.org/10.1021/ma0018143>.
- [77] H. Tsuji, M. Yamasaki, Y. Arakawa, Stereocomplex formation between enantiomeric alternating lactic acid-based copolymers as a versatile method for the preparation of high performance biobased biodegradable materials, *ACS Appl. Polym. Mater.* 1 (2019) 1476–1484, <https://doi.org/10.1021/acsapm.9b00232>.
- [78] M.A. Washington, D.J. Swiner, K.R. Bell, M.V. Fedorchak, S.R. Little, T.Y. Meyer, The impact of monomer sequence and stereochemistry on the swelling and erosion of biodegradable poly(lactic-co-glycolic acid) matrices, *Biomaterials* 117 (2017) 66–76, <https://doi.org/10.1016/j.biomaterials.2016.11.037>.
- [79] J.A. Nowalk, J.H. Swisher, T.Y. Meyer, Influence of short-range scrambling of monomer order on the hydrolysis behaviors of sequenced degradable polyesters, *Macromolecules* 52 (2019) 4694–4702, <https://doi.org/10.1021/acs.macromol.9b00480>.
- [80] J.S. Park, S.K. Kang, A study on surface, thermal and mechanical properties of absorbable PLGA plate, *Int. J. Control. Autom.* 6 (2013) 73–82, <https://doi.org/10.14257/ijca.2013.6.6.08>.
- [81] H. Yin, R. Wang, H. Ge, X. Zhang, Z. Zhu, Synthesis and structure control of L-lactic acid-glycolic acid copolymer by homo-copolymerization, *J. Appl. Polym. Sci.* 132 (2015) 41566, <https://doi.org/10.1002/app.41566>.
- [82] Q. Gao, P. Lan, H. Shao, X. Hu, Direct synthesis with melt polycondensation and microstructure analysis of poly(L-lactic acid-co-glycolic acid), *Polym. J.* 34 (2002) 786–793, <https://doi.org/10.1295/polym.34.786>.
- [83] J. Kasperczyk, Microstructural analysis of poly(*l,l*-lactide)-co-(glycolide) by  $^1\text{H}$  and  $^{13}\text{C}$  n.m.r. spectroscopy, *Polymer* 37 (1996) 201–203, [https://doi.org/10.1016/0032-3861\(96\)81088-3](https://doi.org/10.1016/0032-3861(96)81088-3).
- [84] S.H. Choi, T.G. Park, Synthesis and characterization of elastic PLGA/PCL/PLGA tri-block copolymers, *J. Biomater. Sci. Polym. Ed.* 13 (2002) 1163–1173, <https://doi.org/10.1163/156856202320813864>.
- [85] H.R. Kricheldorf, G. Behnken, Copolymerizations of Glycolide and L-Lactide initiated with Bismuth(III) n-Hexanoate or bismuth subsalicylate, *J. Macromol. Sci. A* 44 (2007) 795–800, <https://doi.org/10.1080/10601320701406997>.
- [86] G. Gorrasí, A. Meduri, P. Rizzarelli, S. Carroccio, G. Curcuruto, C. Pellecchia, D. Pappalardo, Preparation of poly(glycolide-co-lactide)s through a green process: analysis of structural, thermal, and barrier properties, *React. Funct. Polym.* 109 (2016) 70–78, <https://doi.org/10.1016/j.reactfunctpoly.2016.10.002>.

- [87] H. Tsuji, Y. Ikada, Stereocomplex formation between enantiomeric poly(lactic acid)s. 6. Binary blends from copolymers, *Macromolecules* 25 (1992) 5719–5723, <https://doi.org/10.1021/ma00047a024>.
- [88] J. Meimoun, A. Favrelle-Huret, M. Bria, N. Merle, G. Stoclet, J. De Winter, R. Mincheva, J.-M. Raquez, P. Zinck, Epimerization and chain scission of poly(lactides) in the presence of an organic base, *TBD Polym. Degrad. Stab.* 181 (2020) 109188, <https://doi.org/10.1016/j.polymdegradstab.2020.109188>.
- [89] H.R. Kricheldorf, J.M. Jonté, M. Berl, Poly(lactones) 3. Copolymerization of glycolide with L, L-lactide and other lactones, *Makromol. Chem.* 12 (1985) 25–38, <https://doi.org/10.1002/macp.1985.020121985104>.
- [90] B. Lotz, G. Li, X. Chen, J. Puiggali, Crystal polymorphism of poly(lactides) and poly(Pro-alt-CO): the metastable beta and gamma phases. Formation of homochiral PLLA phases in the PLLA/PDLA blends, *Polymer* 115 (2017) 204–210, <https://doi.org/10.1016/j.polymer.2017.03.018>.
- [91] S. Lee, M. Kimoto, M. Tanaka, H. Tsuji, T. Nishino, Crystal modulus of poly(lactic acid)s, and their stereocomplex, *Polymer* 138 (2017) 124–131, <https://doi.org/10.1016/j.polymer.2018.01.051>.
- [92] A. Grivet-Brancot, M. Boffito, G. Ciardelli, Use of polyesters in fused deposition modeling for biomedical applications, *Macromol. Biosci.* 22 (2022) 2200039, <https://doi.org/10.1002/mabi.202200039>.
- [93] S. Targonska, M. Dobrzymyska-Mizera, M. Wujczyk, J. Rewak-Soroczynska, M. Knitter, K. Dopierala, J. Andrzejewski, R.J. Wiglus, New way to obtain the poly(L-lactide-co-D,L-Daltilde) blend filled with nanohydroxyapatite as biomaterial for 3D-printed bone-reconstruction implants, *Eur. Polym. J.* 165 (2022) 110997, <https://doi.org/10.1016/j.eurpolymj.2022.110997>.
- [94] E.H. Backes, E.M. Fernandes, G.S. Diogo, C.F. Marques, T.H. Silva, L.C. Costa, F. R. Passador, R.L. Reis, L.A. Pessan, Engineering 3D printed bioactive composite scaffolds based on the combination of aliphatic polyester and calcium phosphates for bone tissue regeneration, *Mater. Sci. Eng. C* 122 (2021) 111928, <https://doi.org/10.1016/j.msec.2021.111928>.
- [95] E.H. Backes, L. De Nóbile Pires, C.A. Gonçalves Beatrice, L.C. Costa, F. R. Passador, L.A. Pessan, Fabrication of biocompatible composites of poly(lactic acid)/hydroxyapatite envisioning medical applications, *Polym. Eng. Sci.* 60 (2020) 636–644, <https://doi.org/10.1002/pen.25322>.
- [96] R.L. Simpson, S.N. Nazhat, J.J. Blaker, A. Bismarck, R. Hill, A.R. Boccaccini, U. N. Hansen, A.A. Amis, A comparative study of the effects of different bioactive fillers in PLGA matrix composites and their suitability as bone substitute materials: a thermo-mechanical and in vitro investigation, *J. Mech. Behav. Biomed. Mater.* 50 (2015) 277–289, <https://doi.org/10.1016/j.jmbbm.2015.06.008>.
- [97] B. Laycock, M. Nikolić, J.M. Colwell, E. Gauthier, P. Halley, S. Bottle, G. George, Lifetime prediction of biodegradable polymers, *Prog. Polym. Sci.* 71 (2017) 144–189, <https://doi.org/10.1016/j.progpolymsci.2017.02.004>.
- [98] S. Lyu, R. Sparer, D. Untereker, Analytical solutions to mathematical models of the surface and bulk erosion of solid polymers, *J. Polym. Sci. B Polym. Phys.* 43 (2005) 383–397, <https://doi.org/10.1002/polb.20340>.
- [99] A. Schädlich, S. Kempe, K. Mäder, Non-invasive in vivo characterization of microclimate pH inside in situ forming PLGA implants using multispectral fluorescence imaging, *J. Control. Release* 179 (2014) 52–62, <https://doi.org/10.1016/j.jconrel.2014.01.024>.
- [100] T. Fan, W. Ye, B. Du, Q. Zhang, L. Gong, J. Li, S. Lin, Z. Fan, Q. Liu, Effect of segment structures on the hydrolytic degradation behaviors of totally degradable poly(L-lactic acid)-based copolymers, *J. Appl. Polym. Sci.* 136 (2019) 47887, <https://doi.org/10.1002/app.47887>.
- [101] T.I. Croll, A.J. O'Connor, G.W. Stevens, J.J. Cooper-White, Controllable surface modification of poly(lactic-co-glycolic acid) (PLGA) by hydrolysis or aminolysis I: physical, chemical, and theoretical aspects, *Biomacromolecules* 5 (2004) 463–473, <https://doi.org/10.1021/bm0343040>.
- [102] J. Russias, E. Saiz, R.K. Nalla, K. Grym, R.O. Ritchie, A.P. Tomsia, Fabrication and mechanical properties of PLA/HA composites: a study of in vitro degradation, *Mater. Sci. Eng. C* 26 (2006) 1289–1295, <https://doi.org/10.1016/j.msec.2005.08.004>.
- [103] Z. Hong, P. Zhang, C. He, X. Qiu, A. Liu, L. Chen, X. Chen, X. Jing, Nano-composite of poly(*L*-lactide) and surface grafted hydroxyapatite: mechanical properties and biocompatibility, *Biomaterials* 26 (2005) 6296–6304, <https://doi.org/10.1016/j.biomaterials.2005.04.018>.
- [104] Y. Shikinami, M. Okuno, Bioresorbable devices made of forged composites of hydroxyapatite (HA) particles and poly-L-lactide (PLLA): part I. basic characteristics, *Biomaterials* 20 (1999) 859–877, [https://doi.org/10.1016/s0142-9612\(98\)00241-5](https://doi.org/10.1016/s0142-9612(98)00241-5).